AD_____

Award Number:

**W81XWH-09-1-0420**

TITLE:
**High Resolution PET Imaging Probe for the Detection, Molecular Characterization and Treatment Monitoring of Prostate Cancer**

PRINCIPAL INVESTIGATOR:

**Stan Majewski, Ph.D.**

**Neal H. Clinthorne, M.S.**

CONTRACTING ORGANIZATIONS:
West Virginia University Research Corporation
Morgantown, WV 26505

REPORT DATE:
**July 2010**

TYPE OF REPORT:
**ANNUAL**

PREPARED FOR: U.S. Army Medical Research and Materiel Command
Fort Detrick, Maryland 21702-5012

DISTRIBUTION STATEMENT:

[X] Approved for public release; distribution unlimited

# REPORT DOCUMENTATION PAGE

*Form Approved*
*OMB No. 0704-0188*



| 1. REPORT DATE *(DD-MM-YYYY)* | 2. REPORT TYPE | 3. DATES COVERED *(From - To)* |
|---|---|---|
| 01-07-2010 | Annual | 1 JUL 2009 - 30 JUN 2010 |

**4. TITLE AND SUBTITLE**
High-Resolution PET Imaging Probe for the Detection, Molecular Characterization and Treatment of Prostate Cancer

**5a. CONTRACT NUMBER**

**5b. GRANT NUMBER**
W81XWH-09-1-0420

**5c. PROGRAM ELEMENT NUMBER**

**6. AUTHOR(S)**
Neal H. Clinthorne, M.S. & Stan Majewski, Ph.D.

Email: smajewski@hsc.wvu.edu

**5d. PROJECT NUMBER**

**5e. TASK NUMBER**

**5f. WORK UNIT NUMBER**

**7. PERFORMING ORGANIZATION NAME(S) AND ADDRESS(ES)**
West Virginia University Research Corporation
Morgantown, WV 26505

**8. PERFORMING ORGANIZATION REPORT NUMBER**

**9. SPONSORING / MONITORING AGENCY NAME(S) AND ADDRESS(ES)**
U.S. Army Medical Research
and Material Command
Fort Detrick, Maryland
21702-5012

**10. SPONSOR/MONITOR'S ACRONYM(S)**

**11. SPONSOR/MONITOR'S REPORT NUMBER(S)**

**12. DISTRIBUTION / AVAILABILITY STATEMENT**
APPROVED FOR PUBLIC RELEASE; DISTRIBUTION UNLIMITED

**13. SUPPLEMENTARY NOTES**

**14. ABSTRACT**
The goal of this work is to improve methods of molecular imaging for diagnosis as well as treatment planning and monitoring in prostate cancer. This investigation hypothesizes that a dedicated endorectal probe for positron emission tomography (PET) will provide significant improvements in image quality over conventional, external-ring PET scanners used alone. The project is developing prototype high resolution PET detectors that have the possibility of endorectal use and is evaluating potential advantages using phantom studies prior to use in human subjects. Progress to date has been significant with the development of several prototype detectors that achieve desired resolution performance and that will be interfaced to a partial-ring PET system for testing in the upcoming year. Particularly exciting from the viewpoint of developing devices that can be tested clinically was interest in the technology by a major manufacturer of conventional PET instruments.

**15. SUBJECT TERMS**
Molecular Imaging, Positron Emission Tomography (PET), Prostate Cancer

| 16. SECURITY CLASSIFICATION OF: | | | 17. LIMITATION OF ABSTRACT | 18. NUMBER OF PAGES | 19a. NAME OF RESPONSIBLE PERSON |
|---|---|---|---|---|---|
| a. REPORT | b. ABSTRACT | c. THIS PAGE | | | USAMRMC |
| U | U | U | UU | 52 | 19b. TELEPHONE NUMBER *(include area code)* |

## INTRODUCTION

The scope of the research is the investigation of the concept of the dedicated prostate PET imager composed of an endorectal PET probe and a partial PET imager ring operating in a coincidence. The probe placed close to the prostate is a high resolution element of this system, utilizing the magnification PET imaging concept. The University of Michigan team's responsibility is the design and simulation of the concept, construction of the external partial PET ring, and image reconstruction of the resultant laboratory prototype(s) assembled at the University of Michigan. The WVU partner's primary responsibility is in comparative design, construction and validation of the prostate probe based on Silicon Photomultiplier technology. In addition, and beyond the initially defined scope of the first year study, the WVU group performed relevant practical imaging studies using three probe prototypes and planar PET panel detectors, in lieu of a partial ring solution. These results of the first year research are included and discussed below.

There are no anticipated changes to the Statement of Work for the upcoming year. Probes developed at WVU will be interfaced to the partial PET ring at Michigan and evaluated.

## BODY

Agreed Upon Statement of Work

The Statement of Work agreed upon among the participating parties and the granting agency is shown below. Those tasks on which progress was required over this year are shaded in the table.

| *Aim / Task* | *Month (from the start)* | *Contributing/* ***Responsible Party*** |
|---|---|---|
| Aim 1: Probe requirements and modeling (Michigan) | | |
| Refine probe requirements | 1-3 | MP/**NC** |
| Develop Monte Carlo simulations | 1-6 | SH/**NC** |
| Incorporate device measurements from prototypes in Aim 2 | 6-12 | SH/SM/**NC** |
| Develop image reconstruction | 1-12 | SH/**NC** |
| Predict probe performance & evaluate | 3-12 | SH/MP/SM/**NC** |
| Refinements of models, image reconstruction, and performance evaluation methods | 12-36 | SH/MP/SM/**NC** |
| Aim 2: PET probe component selection/validation and prototyping (JLab) | | |
| Technical design selection (options) | 2-4 | JP/NC/**SM** |
| Selection of SiPM modules | 3-4 | JP/**SM** |
| Designing and building prototypes | 5-8 | AS/BK/**SM** |
| Prototype testing | 6-9 | AS/JP/**SM** |
| Technical design selection (final) | 9 | JP/NC/**SM** |
| Aim 3: Probe demonstrator construction/Interface to PET (JLab / Michigan) | | |
| Produce electronics boards | 10-11 | JP/**SM** |
| Assemble SiPMs with electronics | 12 | JP/**SM** |
| Mechanical assembly with enclosure | 10-11 | **BK** |
| DAQ assembly/DAQ software | 6-9 | JM, **JP** |
| Laboratory performance tests / Intrinsic performance evaluation/Attestation | 10-12 | AS/JP/**SM** |
| Interface with PET ring at Michigan | 12-18 | AS/SM/SH/**NC** |
| Performance testing / characterization of | 18-24 | AS/SM/SH/**NC** |

| | | |
|---|---|---|
| probe/ring | | |
| Aim 4: Phantom Imaging studies and performance evaluation (Michigan / JLab) | | |
| Construct phantoms | 12-24 | SH/MP/SM/**NC** |
| Conduct phantom imaging studies | 18-30 | SH/MP/SM/**NC** |
| Compare with performance predictions from Aim 1 | 18-36 | SH/**NC** |
| Summarize Research Results (Michigan / JLab) | | |
| Clinical applicability of prostate probe | 30-36 | MP/SM/**NC** |
| Device designs for next stage | 30-36 | MP/NC/**SM** |
| Determine next funding steps (if any) | 36 | **MP/SM/NC** |

| *Resource* | *Abbreviation* | *Role / Location* |
|---|---|---|
| Neal Clinthorne | NC | PI, Michigan |
| Morand Piert, MD | MP | Co-inv, Michigan |
| Sam Seoung Huh | SH | Graduate Student Research Assistant, Michigan |
| Stan Majewski | SM | PI, WVU |
| James Proffitt | JP | WVU |
| Alexander Stolin | AS | JLab (subcontract) |
| John McKisson | JM | JLab (subcontract) |
| Brian Kross | BK | JLab (subcontract) |

In the next sections, results for each task in the above Statement of Work are summarized. To aid the flow of the presentation, a detailed technical report follows the description of work performed for each task.

**INTRODUCTION CONT'D (WVU REPORT VERSION ONLY)**

We are including here in its entirety the summary report submitted from our collaboration by the leading PI, Dr Neal Clinthorne. In addition, we are commenting on the synergy of the project from the WVU perspective and adding an addendum, which is also a narrative of the new submission for the prostate PET project, which demonstrates how quickly this project produced spin offs and accelerated the potential implementation of the dedicated PET imaging system. Observing our results so far Siemens decided to enter into a contractual agreement with West Virginia University that would enable implementation of our prostate PET probes with their PET/CT scanners. Also, the addendum describes an addition of the biological research part on new more specific prostate imaging agents (by the Johns Hopkins partner) and therefore, it represents almost ideal combination of the advances in biological PET imaging probes and in PET imaging instrumentation systems that will enable, we believe, quick introduction of highly desirable improved imaging of prostate cancer.

Synergy diagram of the effort between UM and WVU, and the spin-off efforts.

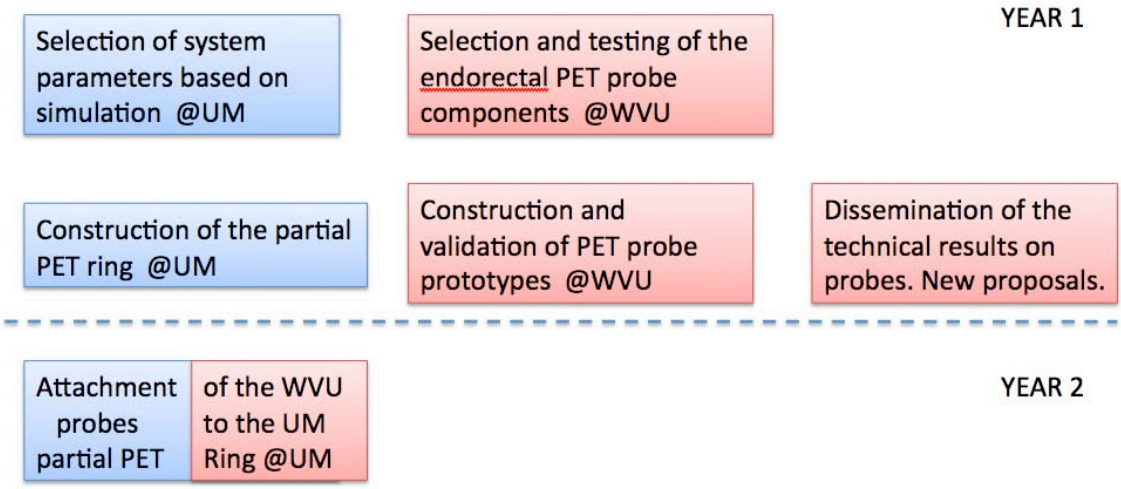


**The diagram above illustrates the synergy in the initial phase of the project. The complementary key efforts of the core project are done in parallel at UM and WVU until the phase when the assembly and operation of the whole system takes place at UM. Due to excellent progress in the technical part at WVU, the side spin-off efforts were initiated early in the process, with new partners interested to be involved in the PET instrumentation, but also in the biological components of the problem to solve (efficient PET imaging of prostate cancer). These additional efforts will be accommodated and expanded through additional funding mechanisms. With the main role and effort of the WVU partner decreasing and the main action moving to UM, WVU can readily get involved in these additional efforts, while providing the necessary full support to the UM partner.**

Aim 1: Probe requirements, modeling, etc.

*Refine requirements*

The probe design used in the original simulations was rather small in size, comprising two 3mm thick layers of a 9 x 35 array of 1mm x 1mm LSO crystals. Consequently, its efficiency was rather limited and it was determined both from discussions with physicians and from the viewpoint that its easier to cut out data to evaluate the performance of smaller probes rather than to not collect that information, we focused on performance of initial sizes of up to 24mm x 40mm x 10mm. It may be feasible, and their may be some advantages to making the 40mm dimension of the probe longer but this will primarily result in an increase in sensitivity. There was some question of whether depth-of-interaction resolution along the 10mm thickness of the probe would be necessary; however, with the demonstration that good depth resolution is possible (Fig. 1), prototypes having depth resolution are being developed.

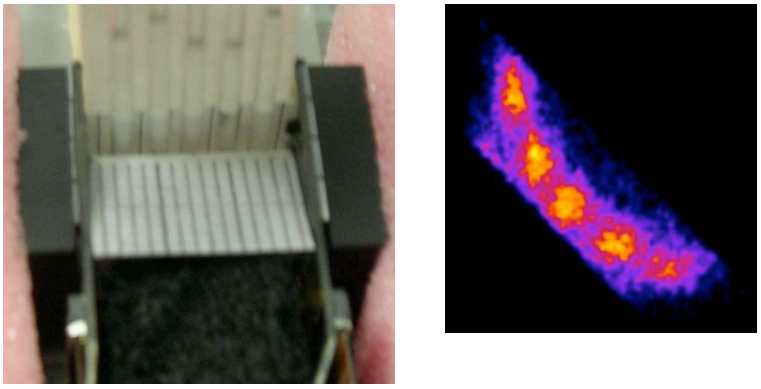

Figure 1. Demonstration of depth-of-interaction resolution in a prototype probe detector consisting of a 2mm x 2mm x 15mm LYSO array read out on both sides by an array of silicon photomultipliers (left). F-18 filled capillary tubes are 2.5mm center-to-center and are well separated in scatter plots where the pulse heights of photodetectors on the right are plotted against those on the left.

Also, as part of the investigation, we hypothesized that high resolution imaging of superficial lymph nodes may be desirable and have proposed additional high-resolution detectors for this purpose. While this is outside the scope of the CDRMP funded investigation, the feasibility and possible benefits of probes for this purpose are being examined as part of an investigation (MADEIRA) funded by the Euratom Program of the European Commission. How such detectors might work in conjunction with the prostate probe and external PET ring is shown in Figure 2.

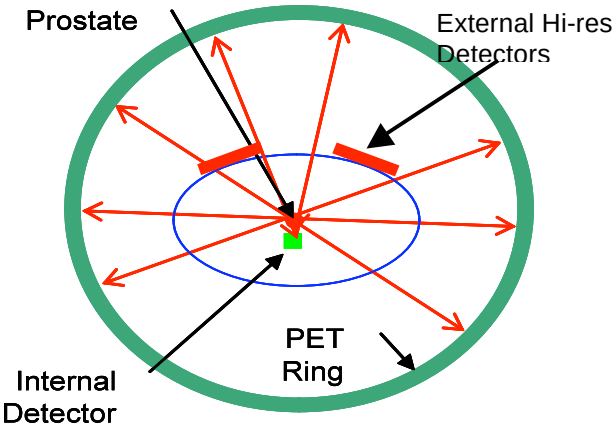


Figure 2: Diagram showing external PET ring, prostate probe and external detectors for high resolution imaging of lymph nodes.

*Develop Monte Carlo simulations*

Monte Carlo simulations for several probe geometries have been developed using the Geant 4 Monte Carlo code. Several internal and external detector arrangements are presently under investigation including the full-ring external PET geometry described in the grant application, as well as geometries having partial external rings. Even though the partial-ring (or more accurately, "incomplete sampling") detector geometries will result in limited-angle tomography artifacts, they may well be useful in PET guided prostate biopsies. As evidence of the synergies of this project, the modeling efforts have led to additional collaborations with Dr. F. Garibaldi of the *Instituto Superiore di Sanitá (ISS), INFN*, Rome, Italy (www.iss.infn.it) for modeling a partial ring external detector + internal detector with time-of-flight capabilities (to be presented as noted in the Reportable Outcomes section). A diagram of the partial-ring geometry under investigation for the time-of-flight studies is shown in Figure 3.

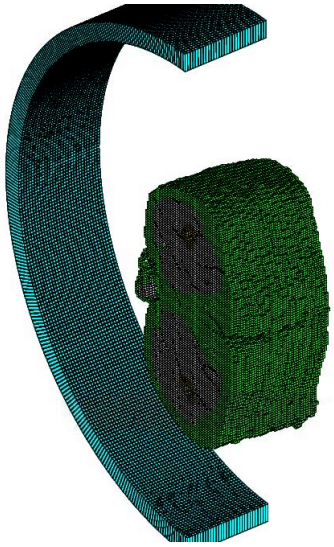

Figure 3: Partial-ring PET geometry being investigated in collaboration with ISS/INFN

Most relevant to the present investigation, however, is the effect on efficiency of using a significantly larger probe than originally reported. Figure 4 shows the efficiency of the 24mm x 40mm x 10mm internal probe compared to that for the smaller original detector. Simulations are presented only for a 15.5 cm axial extent of an 80 cm diameter external PET ring. Just as for the smaller probe, efficiency scales nearly linearly in this regime as the axial extent of the external ring changes. One notes that the number of events recorded by the external ring (green) decreases because relatively more coincidences are captured by the larger internal detector (the yellow triangle is the total sensitivity). The number of events detected by the larger probe increases—not surprisingly—by approximately the ratio of the detector volumes. Expected

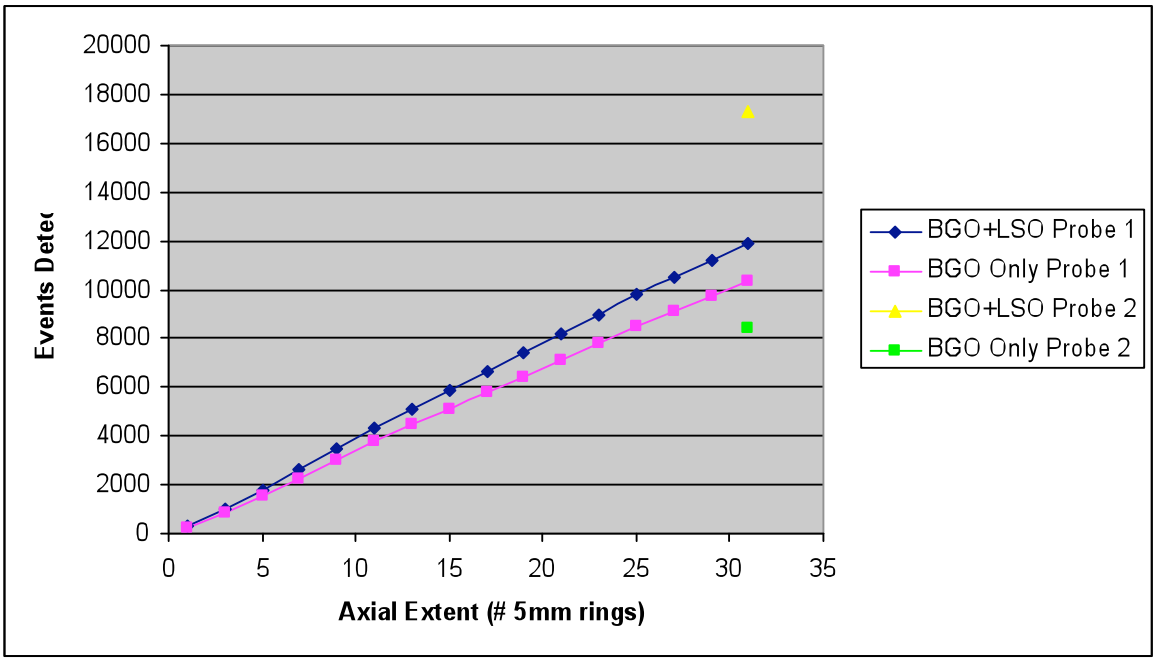


Figure 4. Monte Carlo estimates of efficiency of larger probe in comparison with the original 9 x 35 x 2 array of 1mm x 1mm x 3mm crystals. Note that data detected by external ring (green) decreases as data captured by high resolution probe increases. Total efficiency relative to original system is shown as yellow triangle.

performance in reconstructed images resulting from the increased fraction of high resolution data is examined in a following section.

*Incorporate device measurements from prototypes*

Prototype probes can have several alternative configurations as noted below. We have achieved good intrinsic detector performance with LYSO crystal arrays having dimensions down to 1mm x 1mm x 10mm although there are additional factors that need to be considered for the optimum design such as any tradeoffs in resolution and detection efficiency, in transverse and depth resolution, etc. The most straightforward approach to evaluation will be conducted in the upcoming year when prototype probes developed at WVU are interfaced to the ring system at Michigan. We have, however, examined the sensitivity of the noise-resolution tradeoff in reconstructed images to changes in probe resolution.

To assess performance relative to the originally reported findings, we have performed similar calculations for probes having 1.0mm (original), 1.5mm, and 2.0mm FWHM resolution. Results are plotted in Figure 5. As before, these curves are the ratio of reconstructed standard deviations of the PET ring + probe to the PET ring alone at a given reconstructed resolution. We assume that the intrinsic resolution of the PET ring is 4mm FWHM and that the high resolution information represents ~12% of the total detected events from a point source in the prostate. And as before, one notes that there is little advantage to using the probe if the desired reconstructed resolution is 5mm (or so) or worse; however, as better resolution is desired, all probes demonstrate performance improvements. For example, at 2mm desired resolution in the reconstruction, the probe with an intrinsic resolution of 1.0mm provides a noise equivalent efficiency advantage of 100:1 (the square of the value on the ordinate) over the external PET ring alone. This drops to approximately 16:1 for a probe having 2mm resolution—still a significant improvement. Experiments conducted at WVU over the course the year have demonstrated that resolution close to 1mm is achievable in probes (along with depth resolution of 2 mm to which overall performance is less sensitive).

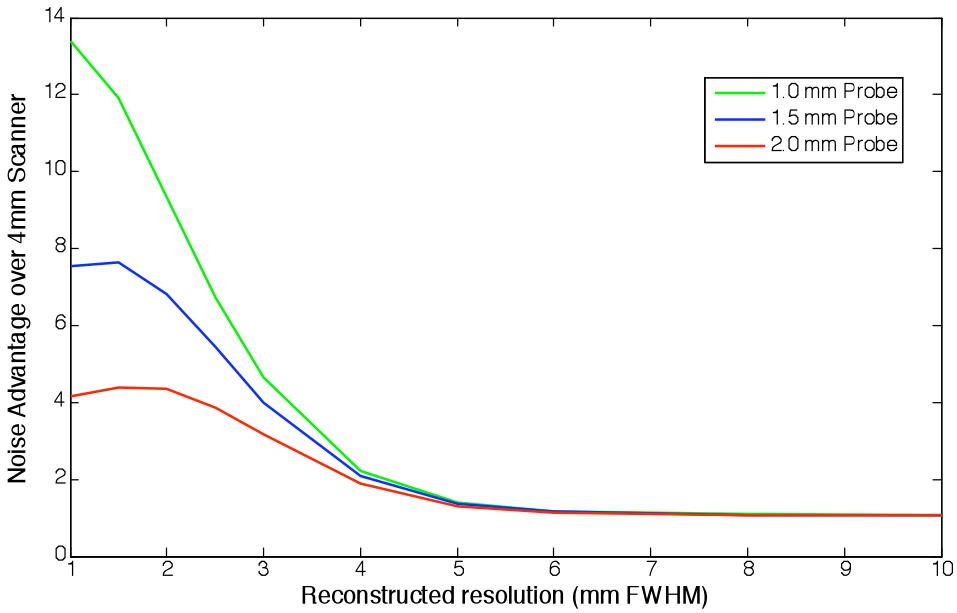


Figure 5. Noise advantage for probes having 1.0mm, 1.5mm, and 2.0mm intrinsic resolution over external PET ring alone. Probes provide additional 12% high resolution data for source in prostate. Intrinsic resolution of external PET ring is 4mm FWHM.

*Develop image reconstruction*

Several reconstruction algorithms are under active development including those used for the limited-angle tomographic reconstructions shown under progress for Aim 2 and algorithms that can potentially be used for real-time reconstruction as might be appropriate for PET guided biopsy. As an example of this latter work, Figure 6 shows a reconstructed mesh plot of two point sources located near a probe. Although the probe used in this case was larger than the prostate probe we anticipate using (50mm x 50mm as opposed to 24mm x 40mm) and the geometry did not sample the object completely (similar to Figure 3), the same algorithm is applicable to reconstructing data from probes to be delivered from WVU in the upcoming year. Importantly, the code has been designed to execute on a graphics processing unit (GPU) with the ultimate goal of realtime reconstruction of 3D probe images. This has been reported in Publication 2 under Reportable Outcomes.

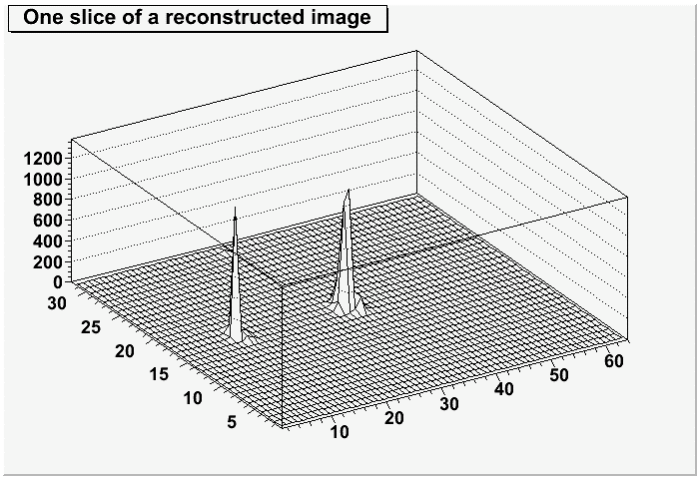


Figure 6. Single slice of a 3D reconstructed image of two point sources located at 10mm and 30mm from the probe detector using a sliding-window list-mode "maximum likelihood' reconstruction method.

*Predict probe performance*

Based on results from Monte Carlo simulations for the probe having the larger detector size, we have recalculated noise advantage over the external PET ring (again with 4mm resolution) and show thre resulting curves in Figure 7. While it is true that efficiency advantages predicted by Monte Carlo can sometimes be difficult to achieve in practice because of factors such as detector deadtime, random coincidences, etc., the noise advantage for the larger detector is ~3x that of the smaller probe (originally modeled design). This translates to a nearly 10x noise equivalent efficiency advantage over the smaller probe, which is more than the simple 5x increase in volume would predict, and illustrates the non-linear benefit of adding high spatial resolution information to data having intrinsically lower resolution.

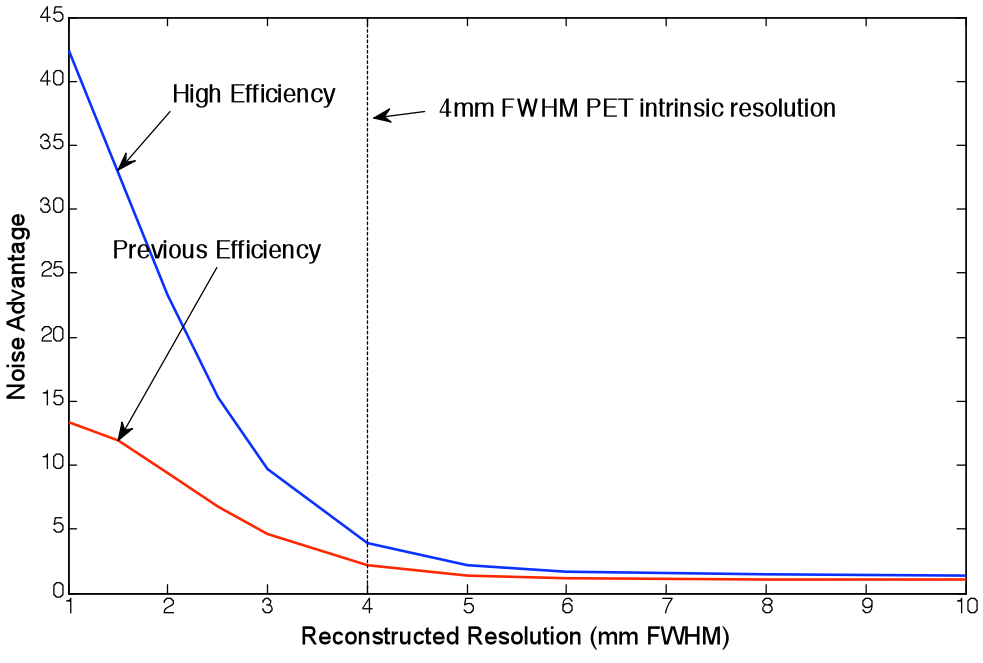

Figure 7: Noise advantage as a function of spatial resolution for two probes. Blue: 24mm x 40mm x 10mm LYSO probe. Red: originally modeled 9 x 35 x 2 array of 1mm x 1mm x 3mm crystals.

Aim 2: Probe component selection and prototype construction

*Partial ring PET system at Michigan*

The probe detectors under development at WVU will be interfaced to a partial ring PET system at Michigan for evaluation. As part of this project, the ring was expanded from 12 to 24 detectors and a flexible FPGA-based interface was developed that should allow for straightforward interfacing of the probes developed at WVU in the upcoming year of this project.

The benchtop system is shown in Figure 8. It consists of 24 BGO block detector modules from a CTI 931 PET scanner along with custom readout electronics. The system shown in Figure 8 has been set up for conducting high resolution PET in a small field-of-view with the aid of silicon detectors. For the upcoming prostate probe experiments, the silicon detectors and mechanics in the center will be replaced with a phantom, the probe, and a computer-controlled turntable so that a full ring of external detectors can be emulated.

The electronics setup for the system (which includes the silicon detectors) is shown in Figure 9. To interface the prostate probe, in principle all that will be necessary is to redesign the logic interface boards to the FPGA module that supply and sequence all control signals, rewrite the FPGA firmware to interface to the WVU probes, and rewrite the data acquisition software. Interface boards for the prostate probe modules essentially replace the silicon detector electronics in the diagram.

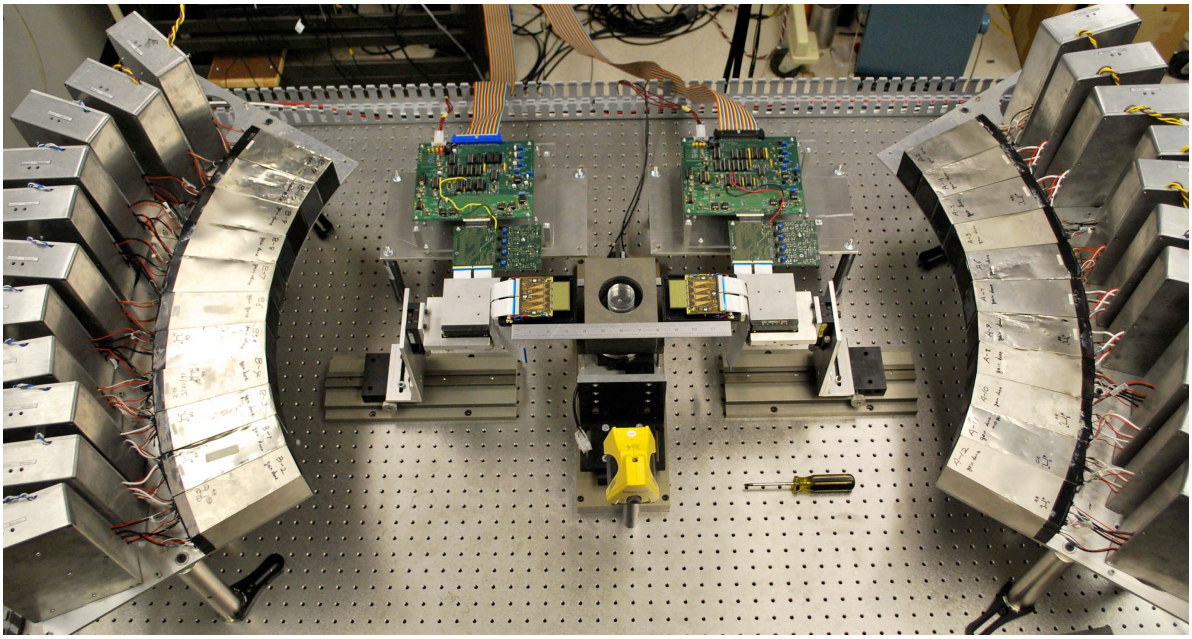

Figure 8. Expanded partial ring PET system at Michigan showing 22 of 24 BGO detector blocks at 500mm radius. System is presently set up to conduct high resolution PET studies with silicon but will be reconfigured shortly to accommodate probe detectors.

*Technical design selection (options)—selection of SiPM modules*

We selected two types of providers for the SiPM sensors: sensL which is providing very compact (<2mm thick) and about 12mmx12mm sensitive modules, and Hamamatsu, which provides the so-called MPPC units of a 3mmx3mm active size. Assemblies of these units form active surfaces of the imaging modules. Unlike sensL devices, there is no limit in size imposed by the MPPC solution. However, sensL devices offer size applicable to the problem of imaging (in a mechanical scan) of the prostate.

*Designing and building prototypes*
The Hamamatsu MPPC arrays were expertly designed (and assembled) by Adaptive I/O Technologies on compact PC board bases, including the on-board fast electronics, offering excellent S/N operation.
The Proteus produced LYSO scintillation arrays, both for single-sided and double-sided DOI operation confirmed to be the best option for the scintillation sensor and all the probes tested were equipped with 1.5mm or 1.0mm granularity arrays.

*Prototype testing*
Three types of detection modules were extensively studied (as described in the attached results below) based on Hamamatsu and sensL devices with the final selection of the Hamamatsu-made variant of the probe for transfer to the University of Michigan. The system includes electronics, data acquisition and computer with calibration and testing software.

*Technical design selection (final)*
Until very recently we have kept both options open for the final probe selection. The last stability issues encountered points to the MPPC solution as being the best choice.

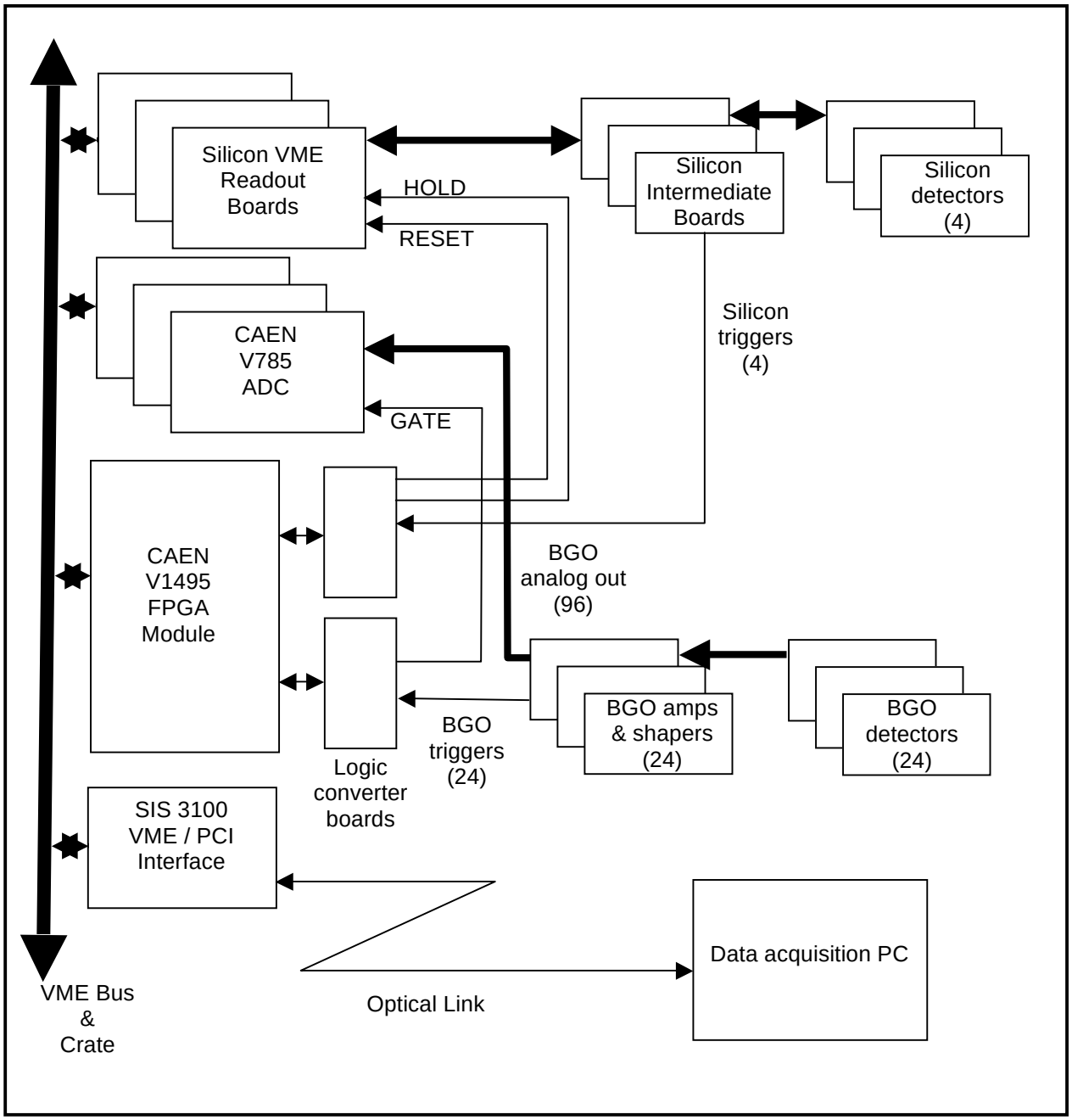


Figure 9. Block diagram of data acquisition system. For prostate probe operation, silicon detectors and associated electronics will be replaced with those necessary to interface to the prostate probe detector electronics.

Aim 3: Probe demonstrator construction

*Produce electronics boards, Assemble SiPMs with electronics*

For the sensLSiPM units, sensL provided fast electronics boards that were operated with the Jefferson Lab DAQ system.

For the MPPC based probes, the on-board electronics and power/cable connect boxes were built by Adaptive I/O Technologies, at the same time when producing MPPC arrays. The arrays were integrated with the PC boards to minimize the package and optimize the S/N performance and reliability.

*Mechanical assembly with enclosure*
For the probe executed with the sensL sensors we had Agile Engineering provide us with a professional compact enclosure and we are continuing tests using this solution. For the MPPC based probes we developed an in-house robust cylindrical shield package to provide compact and flexible arrangement for the performed coincidence imaging studies at WVU with the two prototypes of panel detectors, and for the planned laboratory testing at the University of Michigan.

*DAQ assembly/DAQ software*
The FPGA USB2 fast data acquisition system based on integrating ADCs developed before at Jefferson Lab by James Proffitt (now with Adaptive I/O Technologies) was confirmed to provide the desired high rate capability necessary to operate the probe in a coincidence PET system. The further developed Kmax based data acquisition research software tools, specifically developed for the DAQ modules at Jefferson Lab, were used with the system.

*Laboratory performance tests / Intrinsic performance evaluation/Attestation*
The Technical Report section below extensively describes the tests performed, including additional studies with panel detectors to provide more realistic testing conditions of the probes.

The important final criterion for the selection was the reliability and S/N of the two major technical approaches. While the sensL devices are less expensive and offer higher detection granularity there are serious issues with their reliability and response uniformity. Also their electronics boards and cables developed problems and contributed to the poor and unstable operation. Therefore, our ultimate choice was to provide the University of Michigan with the MPPC based devices. However, we will still continue working with sensL with the hope that the reliability problems will be fixed in the next generation of these otherwise attractive compact devices. We will offer all our probes to the Michigan partner for laboratory testing. The MPPC probes have two sizes (and both will be available for testing). *The final validation of the best choice for the probe will come from the coincidence studies with the partial PET ring imager.*

The immediate challenge will be now how to combine the two elements of the subsystem, after transfer of the probe sub-system to the University of Michigan. However, the probe DAQ system provides time stamp on the recorded events and especially when combined with a fast coincidence trigger, this is expected to be resolved without major difficulties.

<u>Detailed technical report regarding probe hardware</u>

*Introduction: Endorectal magnifying probe approach*
Addition of a high resolution PET probe close to the prostate can convert many PET scanner designs into high resolution prostate PET imager. As far as we know, this concept was first proposed in 1999 by Clinthorne in an NIH grant application aimed at developing a dedicated prostate imager comprising a position-tracked internal detector that worked in conjunction with external “coincidence” Anger cameras in use for PET at the time [1]. The primary focus of the application was for single photon tracers but it was noted that the instrument could be used in for high resolution coincidence imaging of positron emitting nuclides in the same manner as the left diagram in Figure 10. Similar ideas were subsequently presented by Weinberg [2] and independently by Levin [3]. The probe is placed behind the prostate and the outside detector is in front of the prostate and serves as the second coincident detector operating with the probe. The outside detector captures the second, coincident 511 keV gamma ray originating from the positron emissions and annihilations in the prostate and in the immediately surrounding tissue. In this scheme, described also by Moses et al [4] a limited field of view outside of the detector is placed in the fixed position. In this approach, limited detector size and limited angular sampling of the imaging geometry does not allow for full scale, all-angle 3D tomographic imaging of the prostate region and of the surrounding tissue. In contrast, the rightmost diagram in Figure 10, which is based on the idea that a high

resolution internal detector can be used with a standard PET ring, allows complete tomographic data as well as conventional PET imaging to survey for metastatic lesions [5].

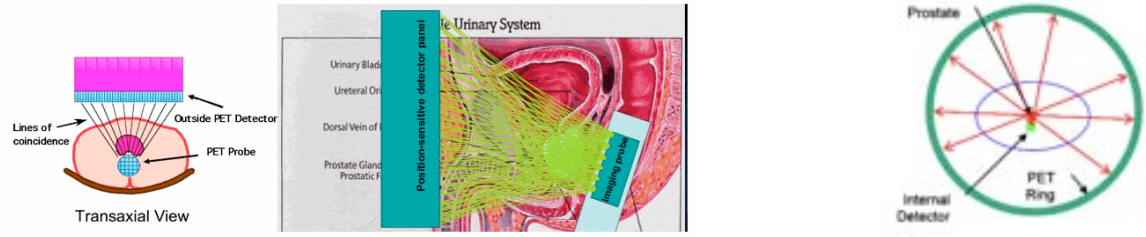


Figure 10. Left: Schematically shown geometry of imaging with an external limited field of view imaging detector placed in front of the patient torso and an endorectal probe placed behind and close to the prostate gland [4]. Center: Closer side view of the two imaging modules shown here with some anatomy details. External detector has a small field of view and is placed very close to the pelvis area. Many examples of coincidence line of response are shown as yellow lines [3]. Right: Conceptual drawing of the (full or partial) PET ring operating in coincidence with a probe [5].

We proposed high resolution probe of 1-1.5 mm intrinsic spatial resolution and 1" x 2" FOV. The novel silicon photomultiplier (SiPM) is the technology we selected for the safe compact endorectal probe detector. Compared to Avalanche Photodiodes (APDs), SiPMs offer much higher gain with much better signal to noise (S/N), simplifying on-board electronics and substantially improving the timing performance. SiPMs also operate at much lower bias voltages than APDs.

*Concept of the probe with DOI capability*

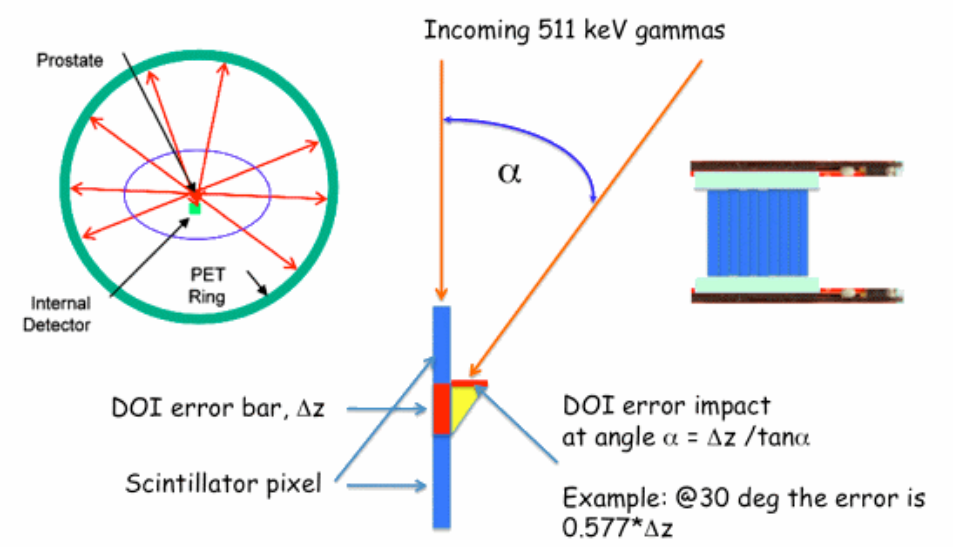


Figure 11. For a range of angles expected in the prostate probe case (top left schematics from Clinthorne et al.) the net effect of limited DOI resolution will be under 1mm. The prostate is assumed to be above the probe with scintillation pixels placed vertically, as pictured at left.

To achieve the desired ~1mm spatial resolution even in the case of limited angle tomography geometry, one needs to measure the depth of 511 keV annihilation photon interactions in the scintillator modules on an event by event basis and use this information in the reconstruction algorithm. Otherwise for photons incident at oblique angles this would lead to parallax error resulting in generation of incorrect LORs contributing to the degradation of spatial reconstruction resolution. Following prior implementations described in the literature, we selected a dual sided readout PET module in which SiPMs are placed at both

ends of a scintillation array and the ratio of the signal from one photodetector (*A*) divided by the sum signal of both detectors (*A*+*B*), as well as the *A*vs*B* plot are used to measure DOI.

*SiPM probe prototypes.*
The PET probes were built based on the SiPM technology. We built and tested three prototypes of the SiPM imaging modules based on MPPC units from Hamamatsu and imaging modules from SensL. The pilot test results are shown below. Our standard multichannel FPGA DAQ system was used to collect the data and Kmaxtoolsheet on a PCto analyze the data.

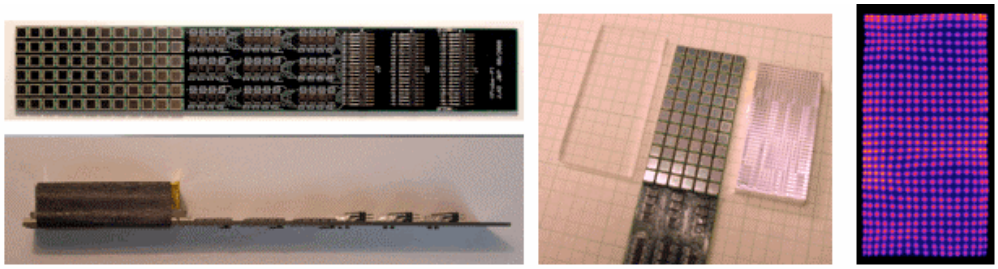

Figure 12. Left: First prototype of a compact full size(3cm wide by 2cm tall) endorectalprostate PET probe (without DOI capability). At left is the photodetector sensor area built out of 72 MPPCs arranged in a 6x12 array. The 3x3xmm MPPC units were spaced at 5mm center to center distance. In the center is the input stage electronics (amplifiers) and at right is the bank of cable connectors matching with three small profile flat cables. Side view of the probe with a 1cm thick LYSO array shows how compact indeed is the design of this SiPM array prototype. The thickness of the total assembly is practically defined by the combined radiation sensor (scintillator) and the light guide. Center: Three key components of the PET probe. Light spreader window provides light sharing between individual MPPC units in the array. Light sharing has to be efficient enough to bridge the dead regions between the MPPC units. LYSO array of 1.5x1.5x10mm pixels (from Proteus).Right: Raw image obtained with the LYSO array coupled to the MPPC array.

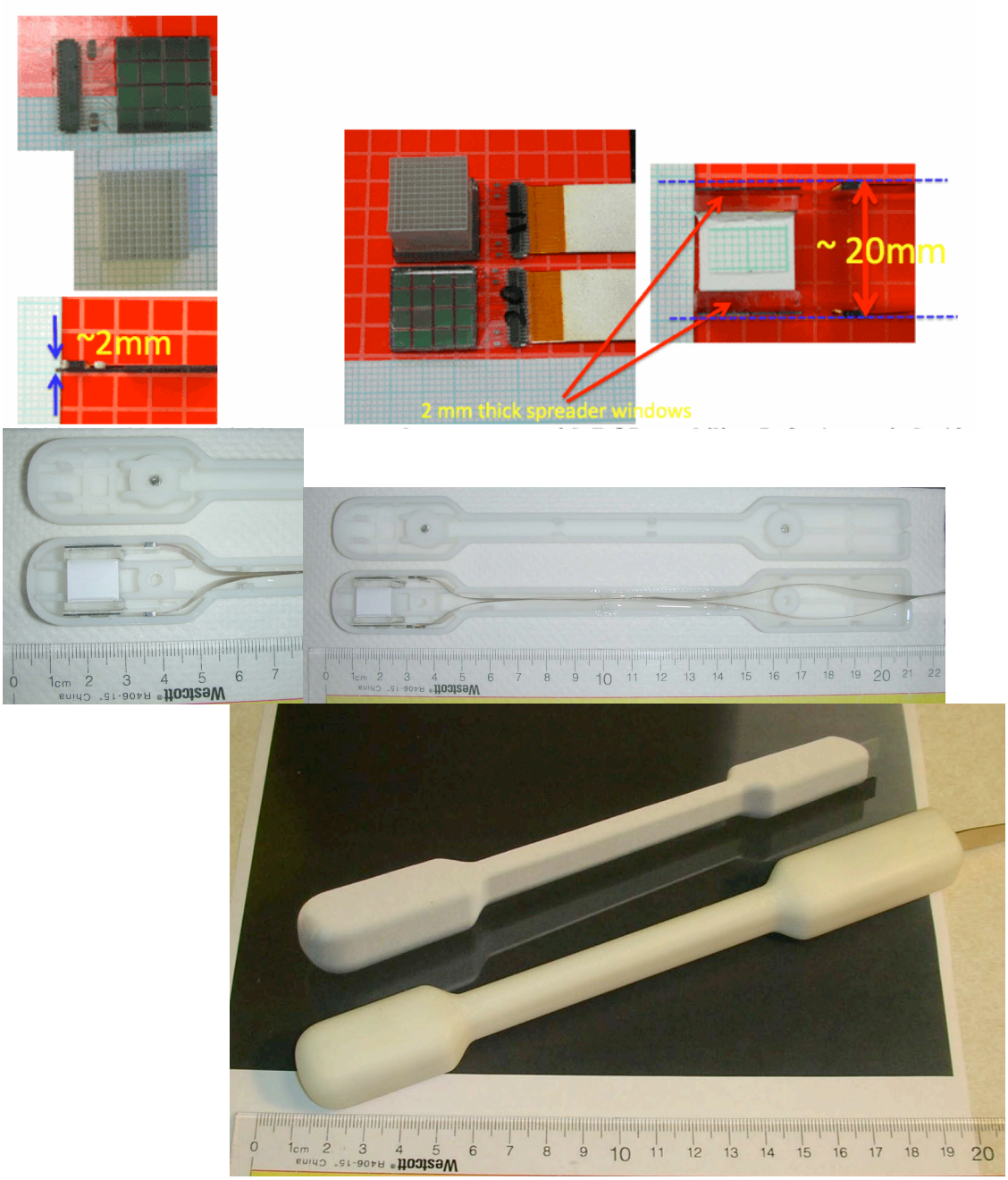


Figure 13. Small size (~14mm wide by ~ 20mm high) prostate probe prototype with DOI capability. Left Top: 1mm pitch, 10mm thick 12x12 pixel LYSO scintillator array from Proteus, with 50 micron Lumirror septa for DOI operation, coupled to the very low profile (<2mm thick) sensL 16ch SPMArray2 module, shown from the top and in a side view. Right Top: 1mm DOI module during assembly with two SiPM modules coupled at both sides of the LYSO array. Glass 2mm thick spreader windows are inserted between the arrays and SiPM modules. Sylgard 3-6636 silicone gel was used as optical coupling between all optical surfaces. Bottom: pictures of the assembled prototype probe with robust mechanical shield to demonstrate the capability of turning the laboratory probe prototypes into practical compact devices.

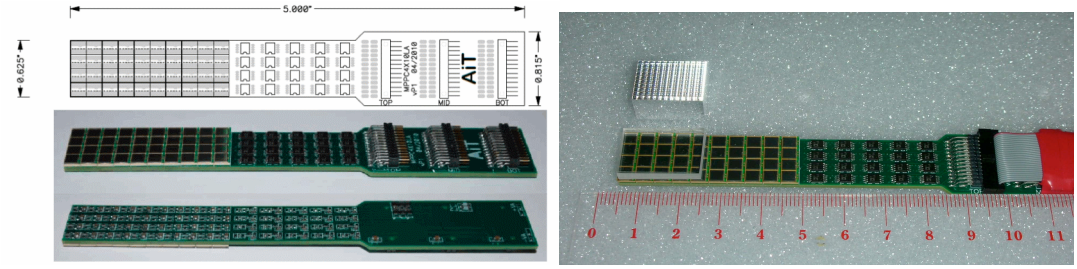

Figure 14. PET probe built by Adaptive I/O Technologies, based on an array of 4x10 MPPC SiPMs from Hamamatsu, with ~ 15mm x 45mm active FOV. Two of these units will read light from two sides of the DOI scintillation array.In the initial trials only the top 16 MPPCs of the probe were read and coupled to the 10x12 pixels of 1.5 x1.5 x10 mm LYSO pixels, or to 16x16 of 1x1x10mm LYSO pixels, both arrays from Proteus. 4.5mm thick acrylic window is used to spread the pixel scintillation light between MPPC pads.

*Studies of the DOI prostate probe prototype.*

Our experimental apparatus consisted of a 12x12 scintillation array with 1x1x10mm$^3$pixels (Proteus) with 50 micronLumirror septa for DOI optimization. The scintillator was optically coupled (Stylgard 3-6636 silicon gel) to two low profile (~1mm thick) 4x4 element SiPMs with 3 x 3mm$^3$ pixels (SPMArray2 from sensL). A 12x12x2mm AR coated UV fused silica light spreader window (Edmund Optics) was placed between both SiPM/scintillator interfaces. FPC cables were used to interface the PET module to custom 16 channel differential pre-amplifiers connected to evaluation/power supply boards (SPMArray2-A0 and SPMArray2-A1 respectively from sensL). Data was acquired via a FPGA-based USB system which has a modular extensible architecture with up to 64 channels of simultaneous sampling ADCs per unit, and a sustained trigger rate of over 150kHz for all channels. A custom designed Kmaxtoolsheet (Sparrow Corp.) was used to analyze the data.

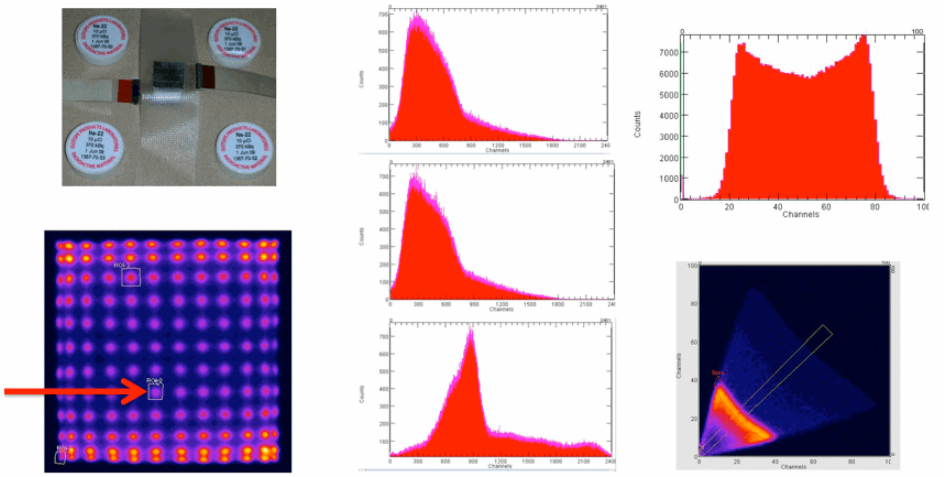

Figure 15. Results obtained with the 1mm DOI module and a broad 511 keV beam from four $^{22}$Na sources. Bottom-left: uncorrected raw image obtained with one of the SiPM modules. All 144 LYSO pixels are visible. One 1x1x10 mm$^3$ LYSO pixel was selected for these studies. Center: energy spectra for the selected LYSO pixel: Output 1 (top), Output 2 (center), Sum (bottom). Top-right: Output 1-to-Sum signal ratio histogram (horizontal scale is in percent). Right-bottom: Output 1 vs Output 2 plot.

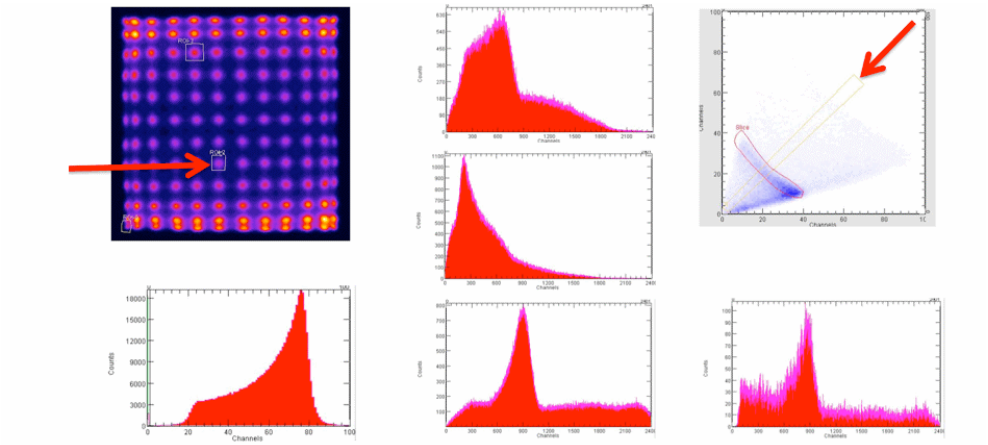

Figure 16. Results obtained with the 1mm DOI module and a broad 511 keV beam from four $^{22}$Na sources. Bottom-left: uncorrected raw image obtained with one of the SiPM modules. All 144 LYSO pixels are visible. One 1x1x10 mm$^3$ LYSO pixel was selected for these studies. Center: energy spectra for the selected LYSO pixel: Output 1 (top), Output 2 (center), Sum (bottom). Top-right: Output 1-to-Sum signal ratio histogram (horizontal scale is in percent). Right-bottom: Output 1 vs Output 2 plot.

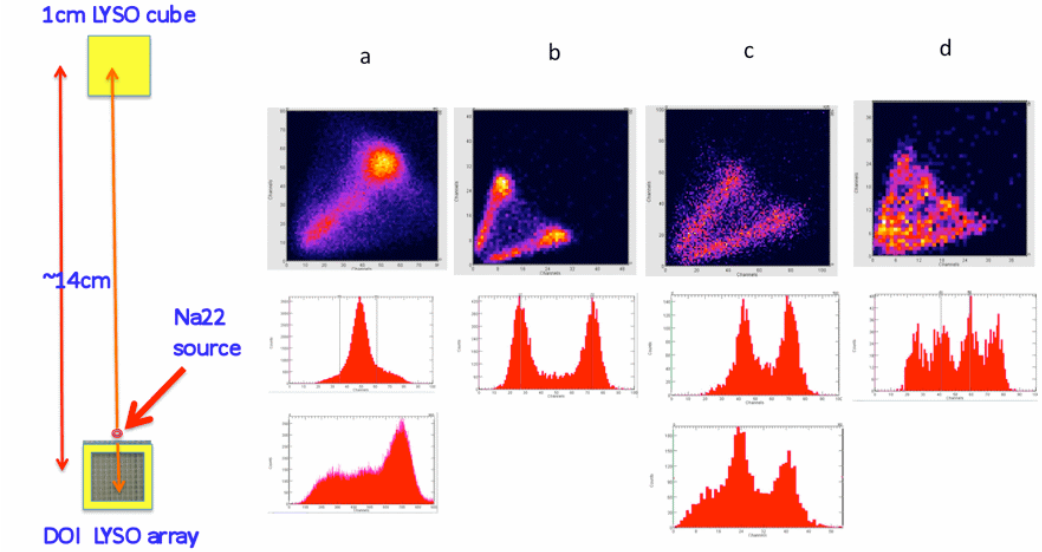


Figure 17. Several measurements of the DOI resolution using Na22 sources and capillaries filled with F18 solution. Electronically collimated beams of 511 keV annihilation rays were produced by using a 1 cm cube LaBr3 crystal mounted to a small PMT as a coincident detector with the 1mm LYSO array, as shown at left. Column a: single 1mm diameter source, b: two Na22 sources placed at 6.5mm, c: two capillaries at 5mm, d: four capillaries at 2.5mm. At top are shown plots of scintillation signals measured for a single LYSO pixel in one SiPM array versus the other (output 1 vs output 2). In the central section are histograms of output 1 vs sum of the two outputs. At bottom are shown energy spectra. Energy spectrum at left is the sum of both outputs for the selected single LYSO pixel. Energy spectrum at right is output 1 for the two-capillary case, showing energy variation with DOI.

*Studies of the dedicated prostate PET imaging systems.*

To evaluate the PET probes at WVU in a coincidence operation, and before transferring the selected probes to the University Michigan, several types of panel detectors were used, as shown below. There was an attempt to evaluate the probes and the setups in geometries simulating the realistic conditions of a prostate imaging scan.

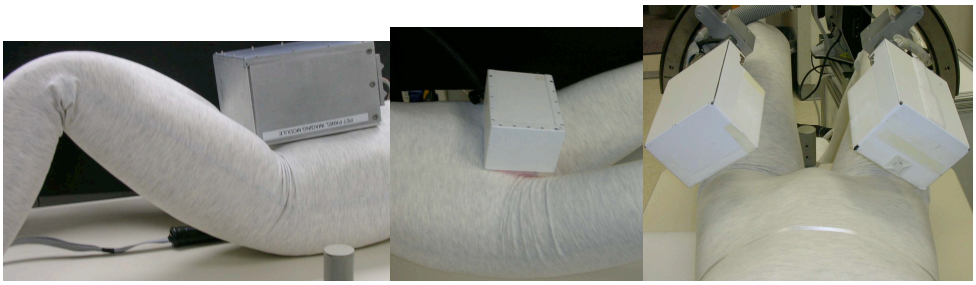

Figure 18. Three variants of the panel detectors used with the probes at WVULeft: 20cm x15 cm active FOV module with 2mm LYSO array, center: 10cm x10cm module with 1.5mm LYSO array, right: stereotactic system with two 10cm modules, made with 3mm LGSO arrays.

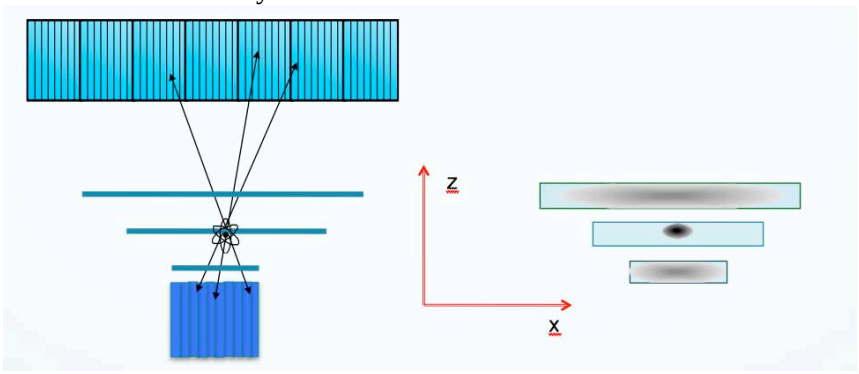


Figure 19. The imaging concept of laminography or focal plane tomography used in the WVU imaging demonstrations of the probe+panel system. The objects are seen "In-Focus" on the object/lesion plane while "Out-Of-Focus" on other planes. The system's advantage is *very* fast reconstruction, but contrast is reduced by out-of-plane activity and spatial resolution In addition, in this case efficiency decreases quickly with distance away from the probe, due to the decreasing acceptance angle.

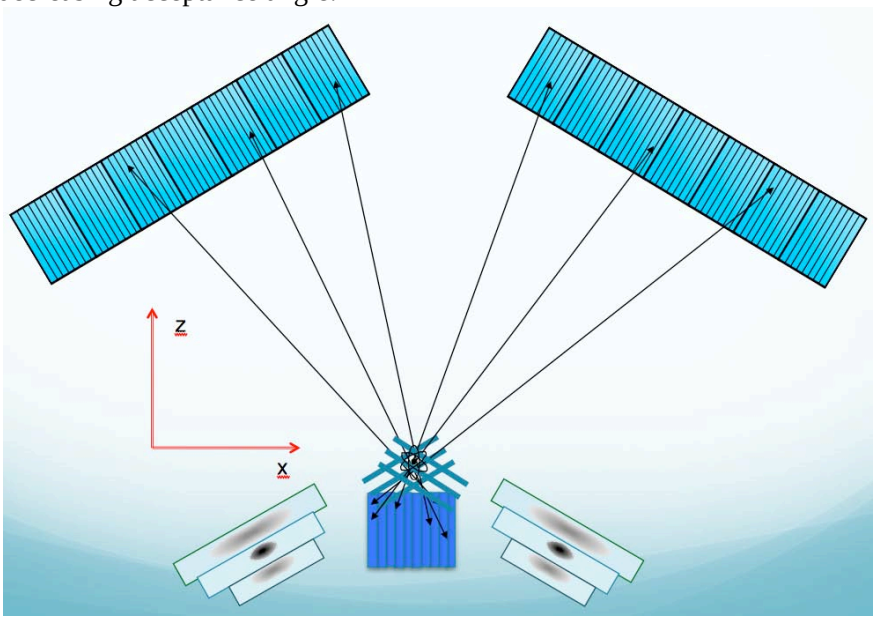


Figure 20. Partial remedy to the depth resolution problem using fast focal plane tomography. The prostate is viewed from two stereotactic directions. The two view will provide enough 3D information to guide biopsy and surgery.

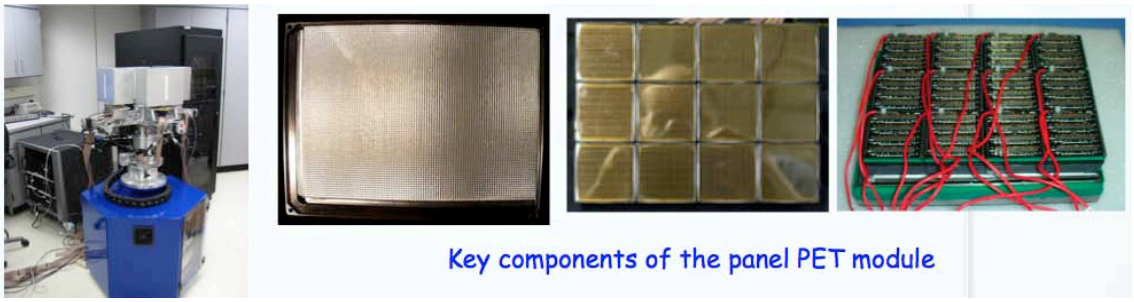


Figure 21. One of the detection modules used before in the PEM/PET WVU breast imager (at left) was implemented as the prostate PET panel detector. An array of 4x3 Hamamatsu flat panel H8500 PMTs was coupled to the Saint Gobain array of 2x2x15mm LYSO scintillator pixels, to form the active FOV imaging surface of about 15cm x 20cm.

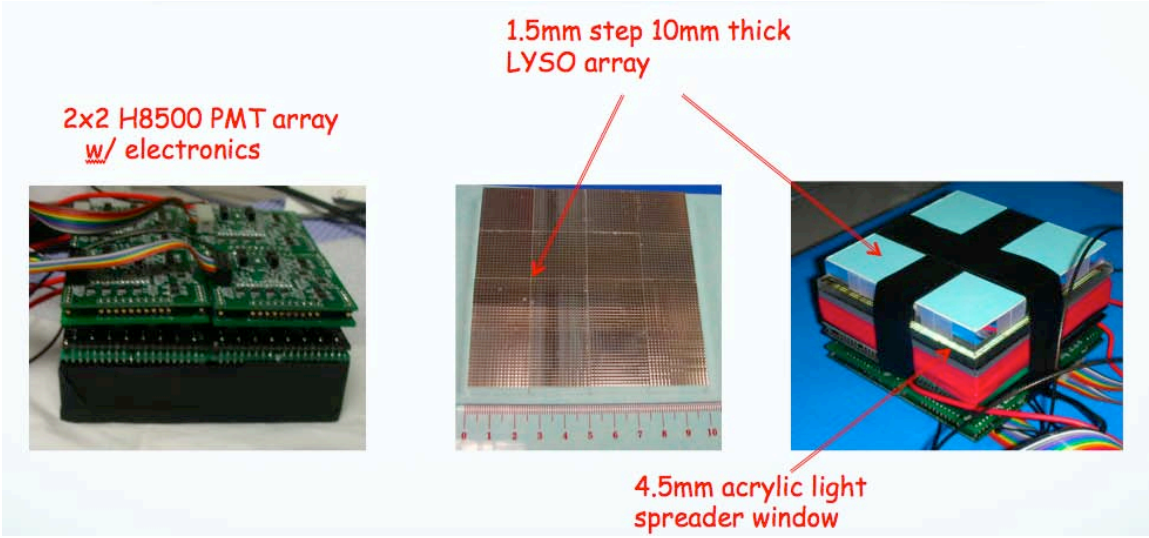


Figure 22. Second smaller ~10 cm FOV panel detector equipped with the 1.5mm step and 10mm thick LYSO array. The LYSO array was built from 16 tiles from Proteus, each with 24 mm x 24 mm active FOV. Scintillator array was coupled to a 2x2 array of flat panel H8500 PMTs to form detector surface with overall coverage of 96 mm x 96 mm. Between the scintillator array and the PMTs a 4.5 mm thick acrylic plate was inserted to provide better scintillation light spreading between the 6mm PMT anode pads. Optical coupling (two component Sylgard 3-6636 Silicone) was used between all optical surfaces.

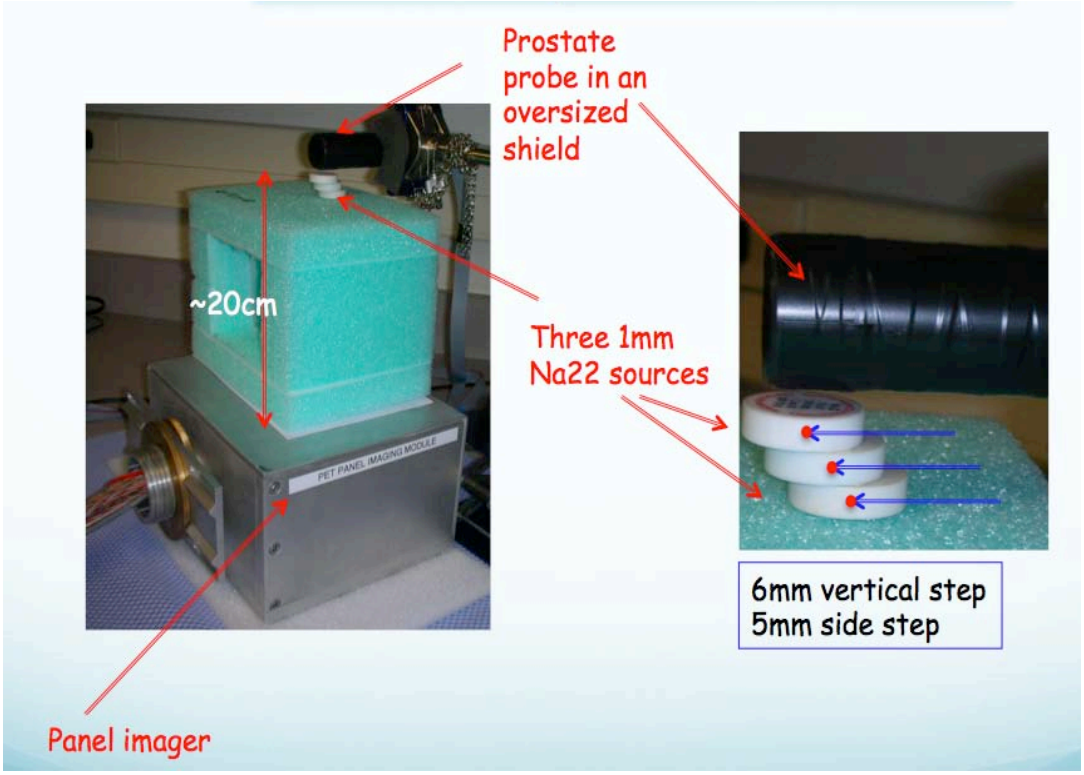


Figure 23. Test setup with the MPPC based probe and a 20x15cm panel imaging module.

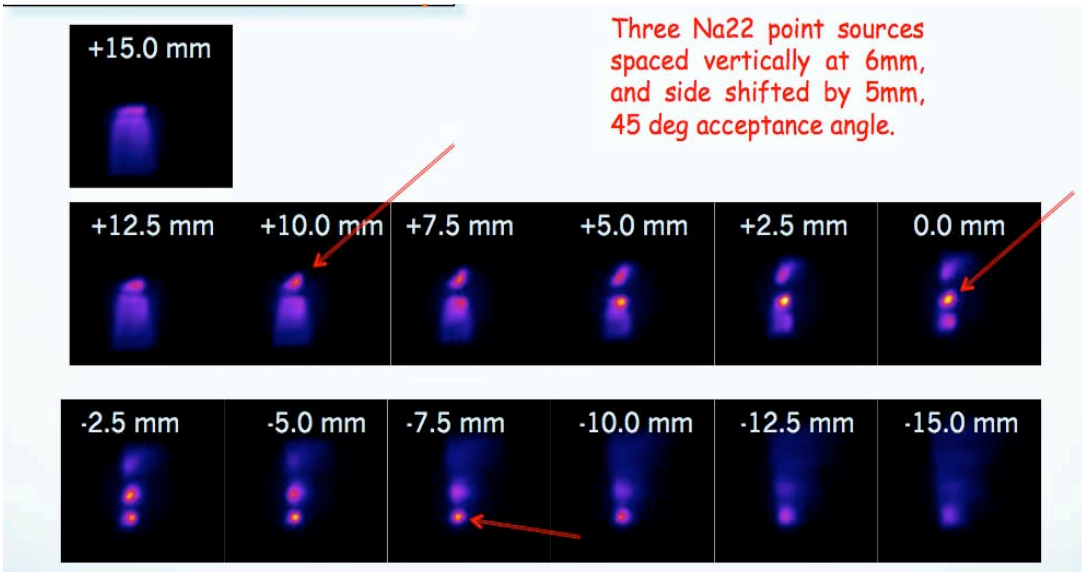


Figure 24. Reconstructed images in thirteen laminography planes spaced at 2.5mm in the z-direction (measured perpendicular to the probe and the panel), and covering z region between -15mm to +15mm from the selected "zero" plane. "Plus" direction is away from the panel imager and towards the probe. All reconstruction angles, limited only by the detector sizes and source geometry, were accepted. Each of the three point sources is best seen "in focus" in one of the planes (marked with red arrows), as expected from the 6 mm vertical (z) spacing of the sources. The planar spacing (seen here in the vertical image coordinate) is 5mm.

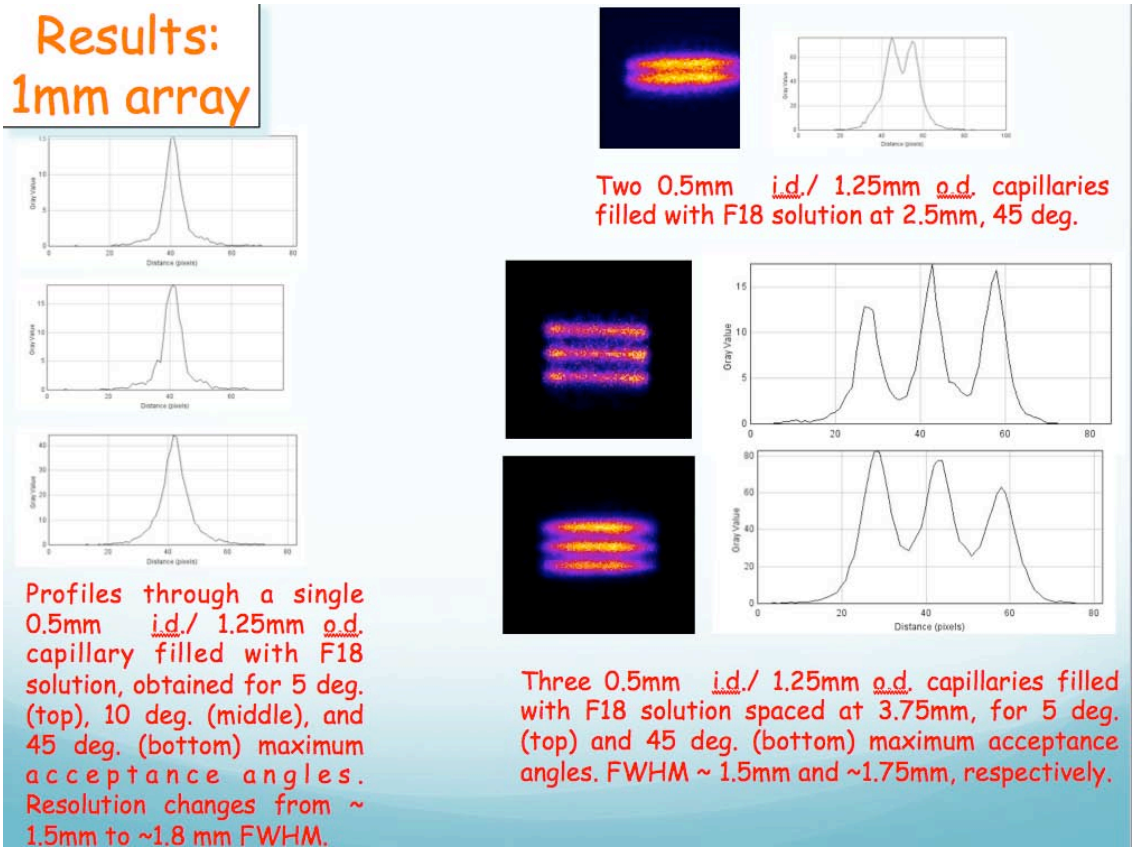


Figure 25. More results from the probe + large panel detector system using capillaries filled with F18 solution.

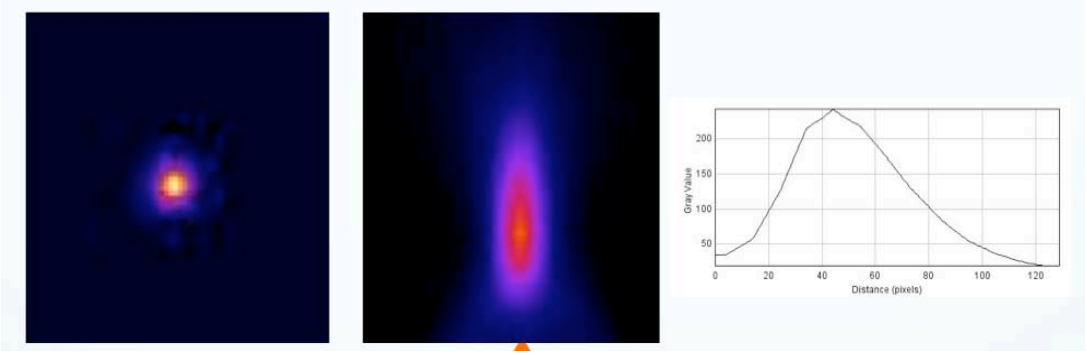


Figure 26. Probe placed close to the large panel detector (at ~5cm distance). Single Na22 point source. 13 vertical (along z coordinate) planes at 1mm spacing (12mm total slice thickness).45 deg. maximum acceptance angle. In-depth resolution is limited when using limited angle tomography. In-plane view in the central plane – location of the point source (left), and the cross-sectional view (center) and plot (at right) obtained in ImageJ from 13 intersection planes, with smooth inter-planar interpolation. Estimated spatial resolution in z coordinate: ~4.7mm FWHM.

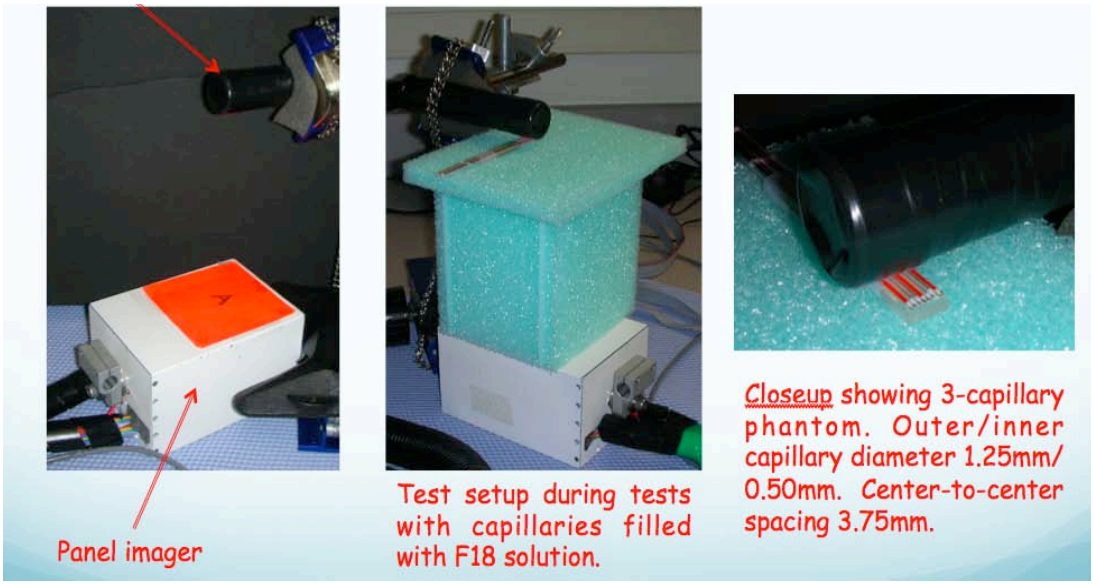


Figure 27. Resolution measurements performed with a panel and a PET probe in a magnified geometry typical of a head/neck focal spot imaging. The probe equipped with a 1mm x1mm x10mm LYSO array covering a 14mmx14mm FOV.

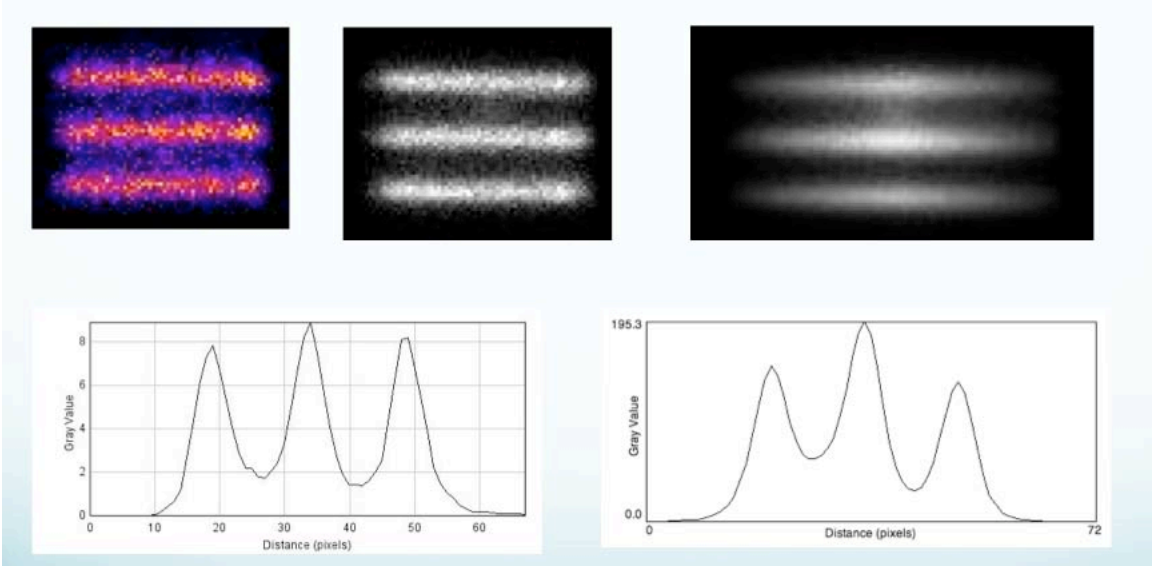


Figure 28. Images obtained with a 3-capillary phantom placed ~1.0cm from the probe. Outer/inner capillary diameter 1.25mm/0.5mm. Center-to-center spacing 3.75 mm. Left: maximum reconstruction angle limited to 5 deg. Spatial resolution 1.35mm FWHM. Right: all angles allowed. Spatial resolution: ~1.65mm FWHM primarily due to DOI effect

From the above probe+panel studies, the conclusions are that indeed the spatial resolution is primarily driven by the performance of the probe, the DOI function is important and that the University of Michigan partial PET ring imager will provide important angular range that in the panel cases was not available. The stereotactic variant of the WVU system was not yet tested, but it will be only an approximation of the partial ring system.

**KEY RESEARCH ACCOMPLISHMENTS**

- Completion of several prototype high resolution probes – testing will begin in year 2 with ring system at Michigan and has already begun using limited-angle "panel" detectors at WVU.
- Demonstration of 3D position resolution capability with crystal arrays read out from both sides using silicon photomultipliers.
- Demonstration of excellent crystal identification in arrays having crystals as small as 1mm x 1mm.
- Preliminary development of GPU-accelerated iterative image reconstruction with the ultimate goal of near real-time 3D images to help guide prostate biopsy.
- Expansion of the partial-ring PET system at Michigan.
- Validation of probes in practical coincidence systems in several configurations with PET panel imagers.
- Interest by Siemens Medical Solutions in testing probes as an add-on existing clinical PET instruments as well as a potential fast-track partnership with Johns Hopkins University in developing new prostate imaging agents.
- A new collaboration with F. Garibaldi to examine the benefit of adding time-of-flight information to the probe both to reduce detected background and to potentially reduce artifacts due to limited-angle tomography.

**REPORTABLE OUTCOMES**

Publications, abstracts, and presentations

1. Clinthorne NH, Majewski S: High resolution PET probe for prostate imaging, Symposium on Intraoperative Imaging, Gargano-Mattinata, Italy, Aug. 28–30, 2009 (Invited)
2. Huh SS, Han L, Rogers WL, Clinthorne NH: Real time image reconstruction using GPUs for a surgical PET imaging probe system. *2009 Nuclear Science Symposium Conference Record*. p. 4148–4153.
3. Studen A, Burdette D, Chesi E, Cindro V, Clinthorne NH, Cochran E, Grosicar B, Honscheid K, Kagan H, Lacasta C, Llosa G, Linhart V, Mikuz M, Stankova V, Weilhammer P, Zontar D: Performance of the MADEIRA PET probe prototype. *2009 Nuclear Science Symposium Conference Record*. p. 3111–3115, 2009.
4. Cochran E, Clinthorne NH, Chesi E, Honscheid K, Huh S, Kagan H, Lacasta C, Mikuz M, Rackers J, Smith S, Studen A, Weilhammer P: High resolution PET using concentric silicon and scintillator rings. *Presented at SORMA XII, May 24 – 28, 2010, Ann Arbor, MI USA.*
5. Garibaldi F, et al, TOPEM: a PET TOF endorectal probe, compatible with MRI and MRS for diagnosis and follow up of prostate cancer, *Accepted for presentation at the World Molecular Imaging Conference (WMIC), September 11–15, 2010 Kyoto, Japan.*
6. Garibaldi F, et al, TOPEM: a Multimodality Probe (PET TOF, MRI and MRS) for diagnosis and follow up of prostate cancer, *Accepted for presentation at the 2010 IEEE Nuclear Science Symposium, Oct. 30–Nov. 6, 2010, Knoxville, TN.*
7. Delfino E, Majewski S, Raylman R, Stolin A: Towards 1mm PET Resolution Using DOI Modules Based on Double-Sided SiPM Readout, *Accepted for presentation at the 2010 IEEE Nuclear Science Symposium, Oct. 30–Nov. 6, 2010, Knoxville, TN.*

8. Huh SS, Cochran E, Honscheid K, Kagan H, Smith S, Rogers WL, Clinthorne NH: The first generation prototype of a surgical PET imaging probe system., *Accepted for presentation at the 2010 IEEE Nuclear Science Symposium, Oct. 30–Nov. 6, 2010, Knoxville, TN*

Other reportable outcomes

9. Potentially the most important outcome is that discussions of the partial results at the 2009 IEEE MIC conference resulted in the WVU group entering into agreement with Siemens Molecular Imaging in Knoxville, TN to embark on the common project in which the WVU partner will design and deliver the PET probe to operate with the Siemens PET/CT scanner. The discussions how to manage the IP created in this project is in the final stages of discussions. The expert Johns Hopkins group lead by Dr Martin Pomper joined the planned effort with the responsibility of developing and providing more specific PET prostate imaging agents to the common effort. The collaboration submitted for a new grant to the prostate program and the narrative of the submission is attached as Appendix 2 below
10. A Michigan Biomedical Engineering graduate student who did much of the initial work on prostate probe evaluation, is developing real-time reconstruction, and alternative high-resolution PET imaging probes is working toward his Ph.D. (expected, Dec. 2010).
11. A WVU physics graduate student is working towards his master's thesis focusing on the experimental aspects of the high resolution prostate probe operation.
12. Three more papers are planned for publication, covering primarily the results with the prostate probe prototypes, but also the results of the laboratory studies of dedicated imaging systems where the probes are combined with panel detectors to form stand-alone mobile imaging system.
13. WVU's urologist/surgeon, Dr Salkini, got interested in the application one of the dedicated prostate PET designed at WVU
14. The Singapore PET group led by Dr David Townsend at the Singapore Bioimaging Consortium got interested in the dedicated prostate PET imaging and the WVU group is assisting with the design of their stereotactic prostate imaging system that will be based on the Singapore developed Silicon PMT arrays. At the invitation of the center, Dr Majewski visited the Singapore in December of 2009 and participated in programmatic discussions, in addition to presenting an invited talk at the one day symposium dedicated to new concepts in PET imaging.
15. There are discussions about accelerating the implementation effort at the University of Michigan by using one of the panel imaging systems developed at WVU in pilot clinical trials at the University of Michigan, while pursuing the development of the proposed system with the partial PET ring, as per the initial plan.
16. As another spin-off of the present effort, WVU, Siemens, University of Michigan, Johns Hopkins and Washington University agreed to submit a common NIH proposal with strong clinical component to validate the concept of imaging prostate cancer with high sensitivity and resolution.

## CONCLUSIONS

Although many of the tasks associated with this investigation will carry over into work for the upcoming year, progress on all fronts was substantial. This was summarized in the Body and Key Research Accomplishments sections of this report. The most exciting development has been interest by Siemens Medical Solutions in the technology with plans for joint grant applications that will provide a fast-track to clinical testing (assuming the appropriate IP details can be managed).

So what?

Based on the studies conducted during the first year of this project, it is likely that:

1. Dedicated PET prostate imagers will provide improved performance over external ring PET alone.
2. Intrarectal detectors having the appropriate performance can be use the detector technology under investigation by WVU.
3. Such a molecular imaging device may be a great help in guiding prostate biopsies.

## REFERENCES

[1] Clinthorne NH: Compton Imaging Probe for the Prostate, NIH Grant R21/33 EB2186, Submitted Nov. 1999, funded Aug 2000–July 2004.

[2] Weinberg IN: Dedicated apparatus and method for positron emission tomography of the prostate, U.S. Pat. No. 7,102,134. Sep. 5, 2006.

[3] Levin C: New Photon Sensor Technologies for PET in Prostate-Specific Imaging Configurations, presented at the Topical Symposium on *Advanced Molecular Imaging Techniques in the Detection, Diagnosis, Therapy, and Follow-Up of Prostate Cancer*, 6-7 December 2005, Rome, Italy, http://www.iss.infn.it/congresso/prostate/presentations_author.htm.

[4] Moses W: Dedicated PET instrumentation for prostate imaging. Presented at the Topical Symposium on *Advanced Molecular Imaging Techniques in the Detection, Diagnosis, Therapy, and Follow-up of Prostate Cancer*, December 6 – 7, 2005, Rome, Italy. http://www.iss.infn.it/congresso/prostate/presentations_author.htm

[5] Clinthorne NH: The Compton prostate probe: promise, recent results, and beyond. Presented at the Topical Symposium on *Advanced Molecular Imaging Techniques in the Detection, Diagnosis, Therapy, and Follow-up of Prostate Cancer*, December 6 – 7, 2005, Rome, Italy. http://www.iss.infn.it/congresso/prostate/presentations_author.htm

## APPENDICES

1. Huh SS, Cochran E, Honscheid K, Kagan H, Smith S, Rogers WL, Clinthorne NH: The first generation prototype of a surgical PET imaging probe system., *Accepted for presentation at the 2010 IEEE Nuclear Science Symposium, Oct. 30–Nov. 6, 2010, Knoxville, TN*
2. Delfino E, Majewski S, Raylman R, Stolin A: Towards 1mm PET Resolution Using DOI Modules Based on Double-Sided SiPM Readout, *Accepted for presentation at the 2010 IEEE Nuclear Science Symposium, Oct. 30–Nov. 6, 2010, Knoxville, TN*.
3. Majewski S, Pomper M, Text of CDMRP Synergistic Idea grant application.

# The first generation prototype of a surgical PET imaging probe system

Sam S. Huh, Eric Cochran, Klaus Honscheid, Harris Kagan, Shane Smith, W. L. Rogers, and Neal. H. Clinthorne

## I. Introduction

PET imaging, measuring function, has unique advantages over other imaging modalities such as MRI and ultrasound that primarily provide anatomical information. As one of the radio-tracers for PET imaging, F-18-FDG in particular has a high avidity for many malignant tumors. As a consequence, PET imaging is gaining widespread acceptance in cancer imaging.

Nevertheless, conventional PET scanners have difficulty in detecting tumors less than 1cm in diameter in clinical use. This problem is due to a variety of factors including background radiation in surrounding tissue, counting noise, and resolution loss due to lack of depth resolution in the detectors. For very small lesions, the relatively large diameter of whole body PET scanners can further degrade the spatial resolution due to annihilation photon acolinearity.

We have been investigating a number of application-specific imaging systems with both high spatial resolution and high sensitivity capability that have laid the basis for the surgical PET imaging probe system. Tai *et al* [1] and Zhou *et al* [2] have been investigating similar application-specific PET devices.

One application we are examining is an intra-operative (surgical) PET imaging probe system. The surgical PET imaging probe is equipped with a position-tracker and is operated in conjunction with a segment of a conventional PET scanner as shown in Fig. 1. Surgeons hold the PET imaging probe and move it around the suspicious regions to collect limited angle tomographic information. Our ultimate goal is to provide a continuously updated 3D reconstructed image that is *re-projected* in real time onto a plane whose orientation is driven by the tracking hardware. In a parallel with ultrasound imaging, the device can be viewed as a handheld, clinician-guided camera capable of seeing the distribution of the radiotracer. This intra-operative PET imaging probe system also can be used for preoperative scans.

For real time image reconstruction, we have investigated an on-line image reconstruction algorithm [3] called Sliding Window OSEM, which is a variant of the one-pass list mode OSEM. We have also implemented the sliding window OSEM on a graphics processing unit (nVidia® GeForce 9800GTX+) to utilize computationally powerful parallel processing [4].

In this paper, we present the first generation prototype of the PET imaging probe system. The prototype consists of a pixelated NaI probe and BGO block detectors. The coincidence circuit was implemented using a programmable VME FPGA (CAEN® v1475). Image reconstruction will be performed on the graphics processing unit using the sliding window algorithm noted above. This study is aimed at demonstrating the feasibility of the PET imaging probe system.

## II. System Configuration

The first generation prototype of the PET imaging probe system consists of a pixelated NaI probe and BGO block detectors. Each NaI pixel measures $2\times2\times10mm^3$. BGO block detectors have $12.5\times5.25\times30mm^3$ cuts. The coincidence circuit was implemented using a programmable VME FPGA (CAEN® v1475)

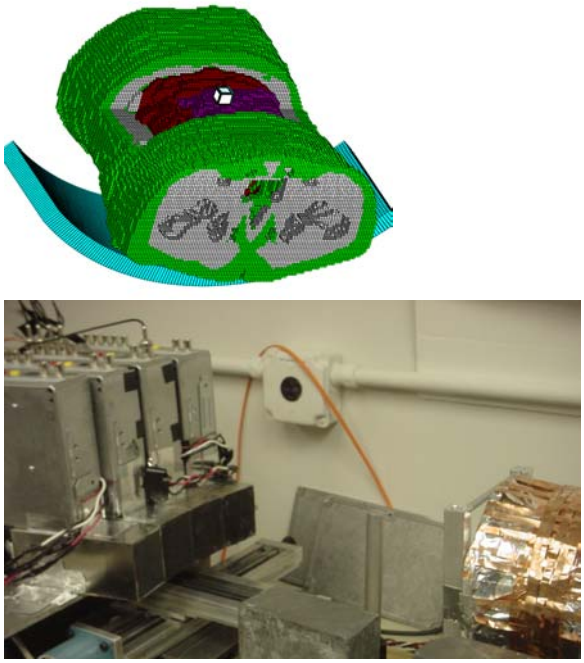

Fig. 1. The illustration of the PET imaging probe system with a partial ring detector and a small probe (the white cube), top picture, and the experimental set-up of the first generation prototype of the PET imaging probe system that shows BGO block detectors (left) and the NaI detector (right), bottom picture.

### *A. The BGO detector*

The BGO block detectors from a CTI 931 PET scanner have a $4\times8$ array of $12.5\times5.25\times30mm^3$ cuts coupled to a $2\times2$ array of 4 25mm square PMTs. Signals from the PMTs are used to estimate interaction positions and deposited energy.

Fig. 2 shows the BGO block detector and the flood image. In order to map the estimated positions to the true positions, the centers of the spots (red dots) were manually selected, then the borders between the spots were drawn. We used the point-in-polygon algorithm to map the estimated position to the true position on the fly.

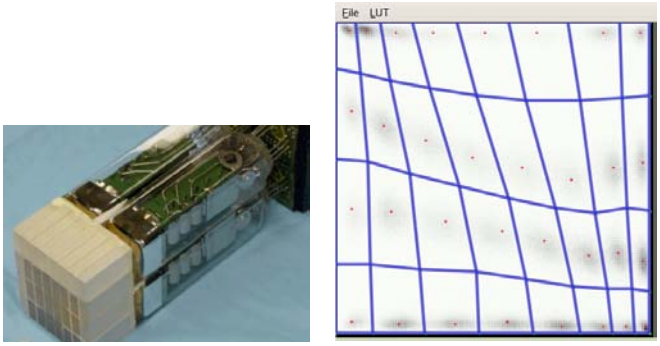


Fig. 2. The BGO block detectors that shows the 4-by-8 array of cuts, left. The flood image of the BGO block detector and the borders between the crystal centers, right.

### B. *The NaI Detector*

The NaI probe (detector) consists of pixelated NaI crystals, a position sensitive PSPMT (Hamamatsu® H8500), a charge division circuit that multiplexes information from the 8 x 8 anode array into four signals, and a front-end readout circuit.

Fig. 3 shows the position sensitive PSPMT with the charge division circuit and a flood image. The whole module is on the NaI crystals. The NaI crystal measures $2\times2\times10$ mm$^3$. The flood image shows that the crystals are well identified around the center. The pitch between the small spots is 2mm.

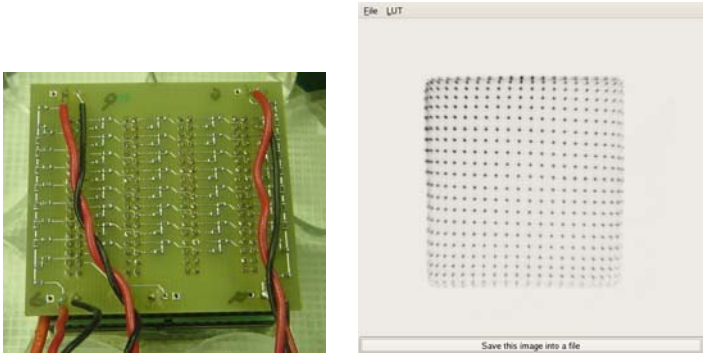


Fig. 3. The PSPMT with a charge division circuit is sitting on NaI crystals, left. The flood image of the pixelated NaI detector, right.

### C. *The coincidence image of a disk with a point source*

The coincidence circuit was implemented using a programmable VME FGPA (CAEN® v1475). The pulse height was digitized using a VME peak sensing ADC (CAEN® v785). The triggers are fed to a delay circuit to align the time delay.

The coincidences between the BGO block detector and the NaI probe were collected using the VME FPGA. We used a disk containing a Na22 (30uCi) point source. The disk was propped up against the NaI detector front surface. Only one BGO crystal was selected for the coincidence data collection. We can select only one BGO crystal using the borders in Fig. 2 and the point-in-polygon algorithm. Fig. 4 shows the VME system we used and the disk with a point source.

Fig. 5 shows the one BGO crystal that is selected to image a single NaI crystal and the estimated position of one NaI crystal. The disk outline was marked in order to map the estimated position to the true NaI crystal position.

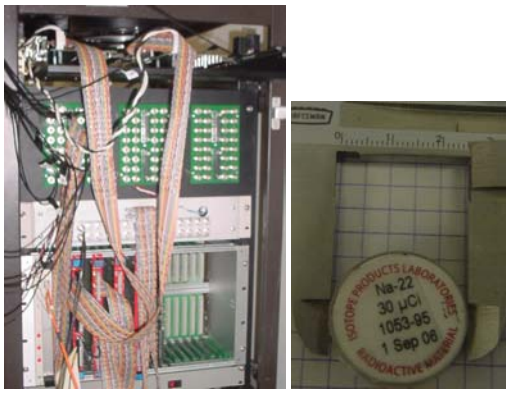


Fig. 4. VME system for coincidence detection and digitizing the pulse height, left. Disk containing a Na22 (30uCi) point source, right.

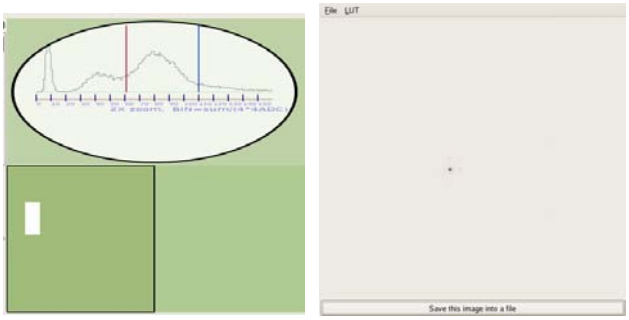


Fig. 5. The selected BGO crystal and the energy spectrum of the BGO detector, left. The estimated position of the single NaI pixel, right.

The real data for image reconstruction will be collected after the mechanical alignment is accomplished. Then a graphics processing unit and the sliding window OSEM algorithm will be used to reconstruct the images from the acquired data.

## III. Discussion and Conclusion

We expect promising results based on the position estimation and the preliminary coincidence data. This study will test the feasibility of the PET imaging probe system.

## References

1. Yuan-Chuan Tai, Heyu Wu, and Marin Janecek, "Initial Study of an Asymmetric PET System Dedicated to Breast Cancer Imaging," IEEE Transactions on Nuclear Science, Vol. 53, No. 1, page(s) 121-126, February.
2. Jian Zhou and Jinyi Qi, "Theoretical analysis and simulation study of a high-resolution zoom-in PET system," Physics in Medicine and Biology, 54 (2009) 5193-5208.
3. S. S. Huh, W. L. Rogers, N. H. Clinthorne, "On-Line Sliding-Window List-Mode PET Image Reconstruction for a Surgical PET Imaging Probe," M13-4 IEEE NSS/MIC/RSTD, October 19-25, 2008, Dresden, Germany
4. Sam S. Huh, Li Han, W. L. Rogers, and N. H. Clinthorne, "Real Time Image Reconstruction Using GPUs for a Surgical PET Imaging Probe System," HPP-13, The workshop on high performance medical imaging (HPMI), NSS/MIC Conference Record. October 25-31, 2009, Orlando, Florida, USA

# Towards 1mm PET Resolution Using DOI Modules Based on Double-Sided SiPM Readout

E. Delfino[1,2], S. Majewski[2], R. Raylman[2] and A. Stolin[2]

[1]Department of Physics, West Virginia University, Morgantown, WV, USA
[2]Center for Advanced Imaging, Department of Radiology West Virginia University, Morgantown, WV, USA

**Abstract.** Parallax error in PET modules can be reduced by measuring the annihilation photon depth of interaction (DOI) in the scintillation crystal on an event-by-event basis. Following implementations described in prior literature, we selected a dual-sided readout PET module design in which SiPMs are placed at both ends of a scintillation array and the ratio of the signal from one photodetector (*A*) divided by the signal sum of both detectors (*A*+*B*), as well as the plot of *A* vs *B* are used to measure DOI. Our experimental apparatus consisted of a 12x12 scintillation array with 1x1x10mm^3 pixels (Proteus) with 50 micron Lumirror septa for DOI optimization. The scintillator was optically coupled (Stylgard 3-6636 silicon gel) to two low profile (~1mm thick) 4x4 element SiPMs with 3x3mm^2 pixels (SPMArray2 from sensL). A 12x12x2mm^3 AR coated UV fused silica light spreader window (Edmund Optics) was placed between both SiPM/scintillator interfaces. FPC cables were used to interface the PET module to custom 16 channel differential pre-amplifiers connected to evaluation/power supply boards (SPMArray2-A0 and SPMArray2-A1 respectively, from sensL). We obtained DOI spatial resolution ~1.5mm FWHM. For the limited instances of parallax error expected in realistic PET systems combined with ~1mm spatial resolution in the scintillation plane, the obtained result for DOI spatial resolution indicates that ~1mm spatial reconstruction resolution PET imaging is possible with the selected technical approach. Applications for such a compact high DOI resolution PET module include a prostate PET probe working in conjunction with a standard clinical PET imager aiding in prostate cancer diagnosis and biopsy guidance, as well as a carotid artery PET probe imaging vulnerable plaque, breast imaging probe, etc.

# Towards 1mm PET Resolution Using DOI Modules Based on Double-Sided SiPM Readout

**Summary.** While positron emission tomography (PET) scanners are becoming increasingly important molecular imaging tools in nuclear medicine[i] many do not measure depth of 511 keV annihilation photon interaction in their scintillators. As a result, the measured position of energy deposition, of the annihilation photons which can travel many millimeters before interacting with the scintillation crystal, is projected to the surface of the crystal. For photons incident at oblique angles this leads to parallax error resulting in generation of incorrect LORs contributing to the degradation of spatial reconstruction resolution. Parallax error can be reduced by measuring the photon depth of interaction (DOI) in the scintillation crystal on an event by event basis and using this information in the reconstruction algorithm.[ii] Following prior implementations described in the literature, we selected a dual sided readout PET module in which SiPMs are placed at both ends of a scintillation array and the ratio of the signal from one photodetector (*A*) divided by the sum signal of both detectors (*A*+*B*), as well as the *A* vs *B* plot are used to measure DOI. While prior publications indicate nearly linear DOI spatial resolution of ~2 mm is attainable[iii] for such a design, we were able to demonstrate that PET modules with DOI spatial resolution ~1.5mm FWHM are indeed possible using specially prepared 1mm LYSO arrays. This improvement in DOI spatial resolution will result in further reduction of parallax error, therefore enhancing the quantitative accuracy of reconstructed images.[iv] For limited parallax errors expected in realistic PET systems, and when combined with ~1mm resolution in the scintillator plane, the obtained result indicates that ~1mm resolution PET imaging is possible with the selected technical approach.

**Apparatus/Method.** Our experimental apparatus consisted of a 12x12 scintillation array with 1x1x10 $mm^3$ pixels [Proteus] with 50 micron Lumirror septa for DOI optimization. The scintillator was optically coupled [Stylgard 3-6636 silicon gel] to two low profile (~1mm thick) 4x4 element SiPMs with 3 x 3 $mm^2$ pixels [SPMArray2 from sensL]. A 12x12x2 $mm^3$ AR coated UV fused silica light spreader window [Edmund Optics] was placed between both SiPM/scintillator interfaces. (**Fig. 1**) FPC cables were used to interface the PET module to custom 16 channel differential pre-amplifiers connected to evaluation/power supply boards [SPMArray2-A0 and SPMArray2-A1 respectively from sensL]. Data was acquired via a FPGA-based USB system [JLab] which has a modular extensible architecture with up to 64 channels of simultaneous sampling ADCs per unit, and a sustained trigger rate of over 150kHz for all channels. A custom designed Kmax toolsheet [Sparrow Corp.] was used to analyze the data.

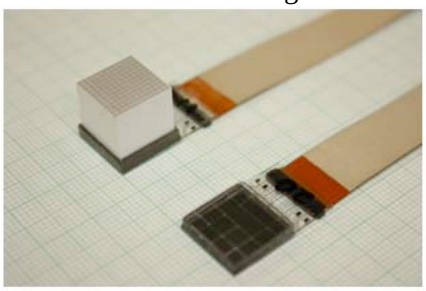

**Fig. 1** (against mm scale background)

**Fig. 2**

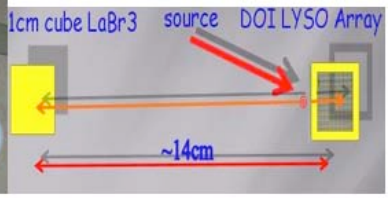


**Fig. 3**

**Results.** Selected results shown here were obtained for a broad 511 keV annihilation photon beam from four 10μCi $^{22}Na$ sources (**Fig. 2**) as well as for an electronically collimated annihilation photon beam from two 50μCi parallel ~0.5mm inner diameter capillaries filled with solution of $^{18}F$. Electronically collimated annihilation photon beams were achieved by using a

second detector using a 1 $cm^2$ PMT optically coupled to a 1 $cm^3$ LaBr3 scintillator operating in coincidence with the DOI module (**Fig. 3**). A single 1x1x10 $mm^3$ LYSO pixel was selected (**Fig. 4)** for the subsequent studies. **Fig. 4** shows uncorrected raw image obtained from a single SiPM array. All 144 pixels are clearly differentiable indicating ~1mm spatial resolution in the plane of the scintillator. **Fig. 5**: Histogram of counts vs. percent ratio of signal *A* divided by the signal sum *A+B*. Distribution symmetry indicates that average signal *A* = average signal *B* as expected for this orientation of sources. **Fig. 6**: Plot of signal *A* vs. signal *B* demonstrating a nearly linear symmetric relationship of signal vs depth in the scintillator.

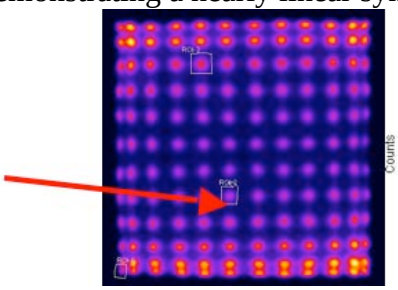

**Fig. 4**

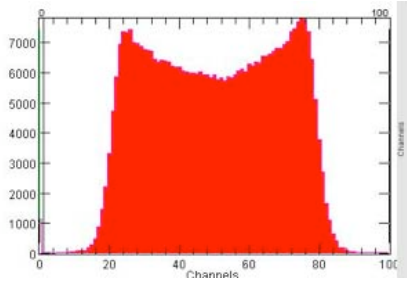


**Fig. 5**

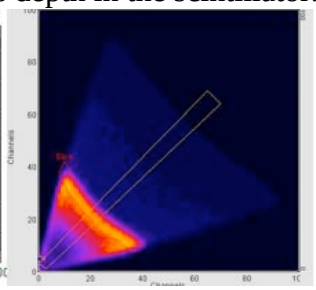


**Fig. 6**

Next, two parallel capillaries spaced at 5mm were placed ~ 1mm from the DOI module. **Fig. 7**: Histogram of counts vs. percent ratio of signal *A* divided by the sum signal *A+B*. We were able to calculate DOI spatial resolution by converting the FWHM of each peak from channels to a physical length. The conversion factor was determined by averaging ratio of the number of channels in the ratio plot to the known associated physical distances (separation between the capillaries). Through this method we were able to estimate DOI spatial resolution of ≤1.5mm FWHM. **Fig. 8**: Plot of signal *A* vs. signal *B*. **Fig. 9**: Histogram of the energy spectrum for a single SiPM (signal *A* only). The two distinct energy peaks demonstrate the variation in energy with respect to DOI.

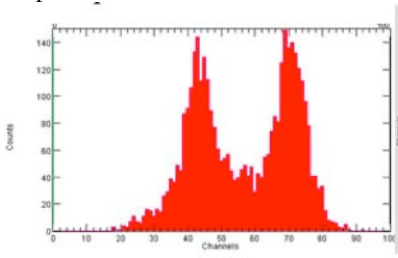


**Fig.7**

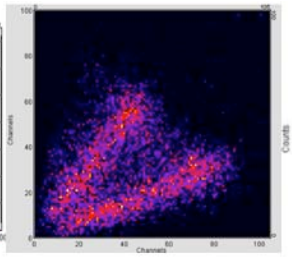


**Fig.8**

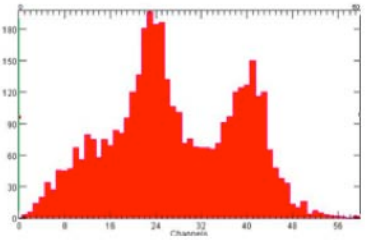


**Fig.9**

**<u>In summary</u>** we have demonstrated that a compact dual-sided readout PET module with ~1mm 2-D spatial resolution and ≤1.5mm FWHM DOI spatial resolution is possible. Demonstration of such a high resolution PET module complements the efforts by others showing that one can limit the effects of the parallax error on the reconstruction image blurring. Applications for such a compact high DOI resolution PET module include a prostate PET probe working in conjunction with a standard clinical PET imager aiding in prostate cancer diagnosis and biopsy guidance, as well as a carotid artery PET probe imaging vulnerable plaque, breast imaging probe, etc.

---

[i] M.E. Phelps, "PET-Molecular Imaging and its Biological Applications", 1st ed., Springer, 2004.

[ii] T.A. DeVol, W.W. Moses, S.E. Derenzo, "Monte Carlo Optimization of Depth-of-Interaction Resolution in PET Crystals", IEEE Transactions on Nuclear Science, Vol. 40, No. 2, April 1993.

[iii] F. Taghibakhsh, S. Cuddy, T. Rvachov, D. Green, A. Reznik, J. A. Rowlands, "Detectors with Dual-Ended Readout by Silicon Photomultipliers for High Resolution Positron Emission Mammography Applications", 2009 IEEE Nuclear Science Symposium Conference Record, pp. 2821-2826, Oct. 2009.

[iv] W.W. Moses, P.R.G Virador, S.E. Derenzo, R.H. Huesman, T.F. Budinger, "Design of a High Resolution, High-Sensitivity PET Camera for Human Brains and Small Animals", ", IEEE Transactions on Nuclear Science, Vol. 44, No. 4, August 1997.

## A. Background

***A.1. Rationale.*** Prostate cancer (PCa) is the leading cancer in the U.S. population and the second leading cause of cancer death in men (1). Therapy for locally advanced disease remains contentious and an increasing number of disparate options are available. More accurate staging would facilitate treatment decisions and lead to a better outcome for patients. In particularly dire need is a way to detect small lesions, i.e., recurrent tumors in the surgical bed, local lymph node invasion and other subtle manifestations of the disease in men with an elevated serum prostate specific antigen (PSA) but no other obvious symptoms. Metabolic imaging techniques such as magnetic resonance spectroscopy (MRS), positron emission tomography (PET) and single photon emission computed tomography (SPECT) are gaining favor over the anatomic techniques of computed tomography (CT) and MR, which merely detect enlarged tissue, revealing nothing of its underlying physiology. Our team is dedicated to building a prostate-dedicated PET imaging device and validating it through use of novel imaging agents that we have recently developed and intend further to develop in this proposal. PSMA is significantly overexpressed in PCa relative to normal prostate tissue (2). With over one million PSMA molecules per cell, it is an excellent target for PCa imaging and therapy. We have recently submitted an application to the FDA to begin using an agent for PET, known as *N*-[*N*-[(*S*)-1,3-dicarboxypropyl]carbamoyl]-4-[$^{18}$F]fluorobenzyl-L-cysteine ([$^{18}$F]DCFBC), which is slated for an immediate human trial (3). Several other experimental PET-based agents are under development, perhaps most prominently those of the choline series, including [$^{11}$C]choline and [$^{18}$F]fluoroethylcholine (4), (5). Another promising, but experimental, PET-based agent is [$^{18}$F]fluorodihydrotestosterone (FDHT) (6), (7). Imaging scientists and urologists are only beginning to implement these compounds for clinical use, with their potential barely realized. Most are designed for imaging metastatic disease – a relatively easy target when compared to intraprostatic imaging, the primary subject of this proposal. Focal therapy for prostate cancer is a subject of intense study and discussion. New, strictly intraprostatic imaging targets are being uncovered, but will lie dormant until there is a way by which to achieve truly high-resolution, intraprostatic molecular imaging. A device that enables study of the molecular characteristics of PCa within the prostate may allow clear delineation of the spread of metabolically active disease into or just beyond the capsule – something not currently possible. It will also provide a way to detect the earliest disease, guide or even obviate biopsy. Perhaps most important, it may enable guidance of focal, minimally invasive therapies. The standard clinical nuclear medicine imagers (gamma cameras, PET scanners) are not optimized for imaging the prostate. These large instruments have suboptimal prostate imaging geometries and insufficient spatial resolutions to separate the signal from surrounding organs. Their sensitivity, spatial resolution, and lesion contrast are inferior to what is potentially achievable with optimized, dedicated prostate imagers and procedures.

The basis of our new concept proposed here is that the new radiopharmaceuticals, offering high target to non-target contrast, can benefit from the proposed high-resolution (~1mm) PET approaches. Standard PET scanners offer spatial resolutions of 4-5 mm at best, which is not adequate to show details of small organs such as prostate. Multimodality imaging offered by standard PET/CT or even magnetic resonance imaging (MRI) + PET is not sufficient due to poor standard PET resolution and poor specificity for cancer of CT and MRI. MR spectroscopy (MRS), another molecular imaging technique, only reports on a limited number of metabolites, indirectly related to malignancy within the prostate, while PET agents can be quite varied and report on the specific pathway under study. And PET is ~100,000 times more sensitive than MRS. The main goal of this proposal is for prostate imaging to be limited by the pharmacokinetics of the radioligand rather than by the intrinsic resolution of the PET scanner. In addition, through the so called partial volume effect, the high resolution also indirectly improves detection sensitivity to small features.

***A.2. Imaging modalities for PCa.***

MRI may improve PCa staging as compared with clinical evaluation alone, CT, or transrectal ultrasound. It allows simultaneous and detailed evaluation of prostatic, periprostatic, and pelvic anatomy. Transrectal magnetic resonance imaging and magnetic resonance spectroscopic imaging (endoMRI/MRSI) allow better visualization of the zonal anatomy of the prostate and better delineation of tumor location, volume, and extent (stage) (8). Metabolic criteria used to identify and localize PCa with endoMRI/MRSI have been standardized, thus improving the accuracy of the examination and limiting inter-observer variations in

interpretation. Evidence is now emerging that endoMRI/MRSI may also be helpful in assessing response to PCa treatment, most commonly with radiation and/or androgen-deprivation therapy. A dual-modality prostate PET imager with transrectal ultrasound (TRUS) was constructed at LBNL Berkeley (9). TRUS provides anatomical detail that can be co-registered with the PET image. This PET imager was constructed from sectors of a standard ECAT HR+ PET with spatial resolution limited to ~4-5mm FWHM. The geometry was closer than standard ring sector geometry, which introduces additional depth of interaction error. The concept of high-resolution PET imaging in the pelvis region with dual planar detectors has been investigated previously in phantom tests by the Duke/Jefferson Lab team (10). The scanner consisted of two 20 cm x 15 cm (axial) planar detectors made of 3mm x 3mm x 10mm LGSO scintillator detection elements. The detector heads were mounted on a rotating gantry with adjustable detector radii. As stated in the final conclusions of that study, the system worked satisfactorily, even with limited views, for detection of high-uptake lesions. Detection of hot lesions in the pelvis with small dual-planar PET detectors was judged to be possible but better characterization of such lesions requires orbiting (or larger) detectors.

### *A.3. Transrectal/endorectal magnifying probe approach*

Addition of a high resolution PET probe close to the prostate can convert many PET scanner designs into high resolution prostate PET imager. A transrectal high resolution (~1mm) prostate PET probe operating in conjunction with a small field of view imaging detector placed by the pelvis and close to the prostate was proposed by Weinberg (11) and independently by Levin (12). The probe is placed behind the prostate and the outside detector is in front of the prostate and serves as the second coincident detector operating with the probe. The outside detector captures the second, coincident 511 keV gamma ray originating from the positron emissions and annihilations in the prostate and in the immediately surrounding tissue. In this scheme, described also by Moses et al (13), a limited field of view outside of the detector is placed in the fixed position. In this approach, limited detector size and limited angular sampling of the imaging geometry does not allow for full scale, all-angle 3D tomographic imaging of the prostate region and of the surrounding tissue.

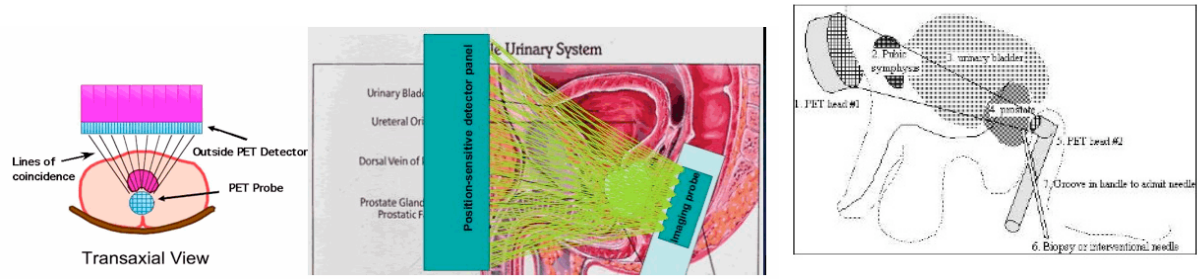


**Figure 1. Left: Schematically shown geometry of imaging with an external limited field of view imaging detector placed in front of the patient torso and an endorectal probe placed behind and close to the prostate gland (13). Center: Closer side view of the two imaging modules shown here with some anatomy details. External detector has a small field of view and is placed very close to the pelvis area. Many examples of coincidence line of response are shown as yellow lines (12). Right: Conceptual drawing of endocavitary PET scanner for prostate (11). Camera head external to body (#1) forms a detector pair with handheld endocavitary camera (#5) on opposite side of prostate (#4). The endocavitary head can be affixed to an ultrasound camera, and can also admit a needle for biopsy or energy delivery for minimally invasive interventions (#6,#7). To reduce singles rate, the bladder (#3) can be drained via a catheter.**

In a hybrid system studied in (14) the authors performed a simulation study of a high-resolution imaging probe in coincidence with a conventional external PET scanner. The internal detector provides both high resolution (~1mm FWHM) and high efficiency while events recorded by the standard PET provide complete tomographic data for image reconstruction. This concept is still under simulation investigation to estimate the performance in comparison with conventional PET. In this case the main issue is how to include the extra coincident endorectal probe in a standard commercial PET/CT imager system. This requires a close collaboration with a particular PET scanner producer to solve the nontrivial technical issues, and this is what we are proposing in this grant submission.

## B. Objective

The goal of this project is two-fold: (1) develop high resolution and high sensitivity PET imagers to image the prostate, and (2) to synthesize and validate new PET-based molecular imaging agents using at least one of the imaging systems developed in (1). The new imaging methods will be benchmarked against imaging with the modern conventional PET/CT scanner, such as the Biograph mCT from Siemens.

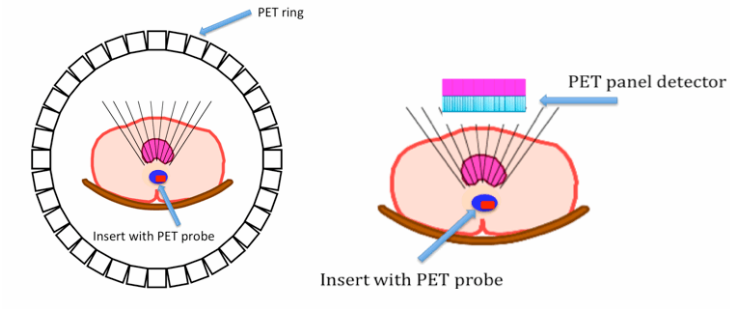


**Figure 2. Left: PET ring (from the PET/CT scanner) operating with the PET probe insert. The PET probe is inserted in a shell insert that enables stabilization of the prostate during procedure. In this example the probe size is narrower than the shell, and side scanning will be performed to zoom-image the particular ROI in the prostate. Right: The dedicated PET concept: PET probe inserted in the shell-insert operating with the external PET panel module. Both modules built on the MR compatible SiPM technology (with minimum impact on MR operation, by design).**

There will be two full instrumentation systems as outcome of this work: a dedicated PET camera and PET/CT scanner with high resolution. In order to achieve this, two PET imaging modules will be developed under this grant: a high resolution compact endorectal PET probe, and a high resolution panel PET imaging module. These additional modules will either operate as: the stand-alone two-component PET imaging system, or be used as inserts in the PET/CT scanner. The operation of the dedicated system (probe+panel) will be compared with the operation of the PET/CT+probe system.

The probe will work as a “magnifying” (15,16,17,18) attachment to the standard PET/CT scanner that will improve the local spatial resolution and increase sensitivity of the PET scan of the prostate. Therefore, dedicated prostate imaging and biopsy guidance can be added to standard PET/CT protocols, as needed. This fully novel application has the potentiality to reach a large install base of existing PET/CT scanner. The addition of Siemens Healthcare Molecular Imaging partner to the present team offers this unique opportunity to expedite the implementation of this concept.

We will construct the compact endorectal high resolution PET probe (FWHM of 1.0-1.5 mm) based on the recent experience acquired at West Virginia University (WVU) in developing SiPM based imagers for different, mostly surgical, applications. SiPM technology offers unique features ideally suited for the system with which this proposal is concerned, including compact size, high gain, low operating voltage, high spatial resolution. The SiPMs are also immune to high magnetic fields, such as those used in MRI. Initial performance tests with several probe prototypes have provided very encouraging results that demonstrate the maturity of this technology for the proposed application.

At the end of the project, the deliverables will be:

- attachment gear for the insert PET modules with the first focus on prostate probe, but transferable also to other inserts for imaging breast or head/neck;
- reconstruction algorithm installed on a work station (not yet on the Siemens scanner) for the operation of the probe with PET/CT scanner (with both functions, PET and CT);
- report/paper on the operation comparison between the PET/CT scanner with the PET insert probe in task specific preclinical tests with realistic phantoms
- dedicated stand-alone PET imager with installed reconstruction algorithm for imaging of the prostate: probe + panel
- report/paper on the operation comparison between the PET/CT scanner with the probe versus the dedicated imager: relative advantages, limitations, in task specific preclinical tests with realistic phantoms
- new prostate specific PET imaging agents ready for clinical trials

In summary, we will prepare all elements necessary to allow under the next immediate funding mechanism to do clinical trials with new improved prostate imaging agents AND new high-resolution PET imaging systems.

## B.1 The dedicated prostate PET imager

The dedicated system has three major components: (1) an external high resolution PET imager module (panel imager) placed close to the patient's pubic area, (2) a compact endorectal PET probe that is placed close to the prostate and operates in conjunction with the external PET module, and a (3) probe location system attached to the PET probe and the panel, to assist with keeping control of relative positioning of the PET probe relative to the prostate gland.

The two PET components of the dedicated detector system (external PET panel and endorectal PET probe) are spatially co-registered to each other via positioning systems installed on both modules. The compact external PET panel imager will be mounted on a flexible mounting arm system. The endorectal PET probe operating in coincidence with the panel imager is placed close to the prostate and by this it provides high sensitivity and high resolution but only a limited 3D view (mostly 2D view) of the region of the prostate. The probe can also provide more precise direct local biopsy or surgery guidance, however this is not proposed in this submission. The probe is large enough to assist with the biopsy guidance and cancer removal, but in most cases is not large enough to be able to image the whole prostate, especially in cases of enlarged prostate where imaging of the whole organ would be practically not possible within the anatomical limits and with acceptable patient comfort level.

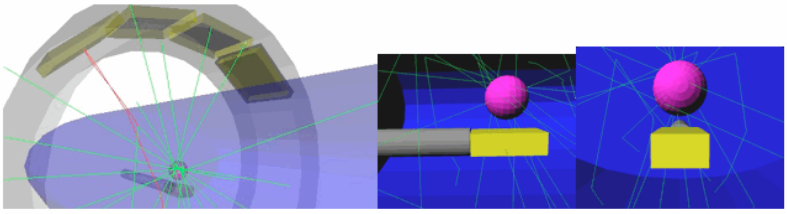

**Figure 3. Another discussed variant of the PET panel imager. The panel detector is made out of four smaller modules in this implementation example. Torso is schematically drawn as a cylinder and prostate is approximated by a sphere. The prostate PET probe is placed under the prostate.**

No examples of prostate probes are available in the literature, but in the course of our development studies at WVU we have produced several prototypes of imaging surgical probes based on SiPM technology. Some of these designs are shown here, and the relevant test results obtained with one of the probes are described elsewhere in this submission.

### *B.1.1 Endorectal probe PET module.*

High resolution probe of 1-1.5 mm intrinsic spatial resolution and 1" x 2" FOV is proposed. The novel silicon photomultiplier (SiPM) is the technology we selected for the safe compact endorectal probe detector. Compared to Avalanche Photodiodes (APDs), SiPMs offer much higher gain with much better signal to noise (S/N), simplifying on-board electronics and substantially improving the timing performance. SiPMs also operate at much lower bias voltages than APDs.

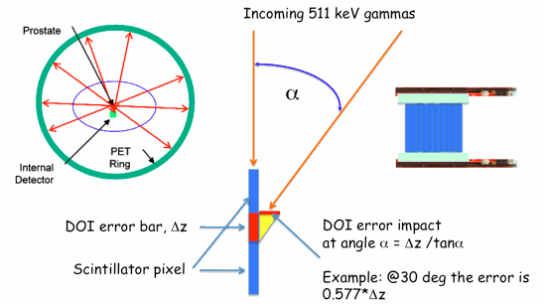


**Figure 4. For a range of angles expected in the prostate probe case (top left schematics from Clinthorne et al.) the net effect of limited DOI resolution will be under 1mm. The prostate is assumed to be above the probe with scintillation pixels placed vertically, as pictured at left.**

To achieve the desired ~1mm spatial resolution even in the case of limited angle tomography geometry, one needs to measure the depth of 511 keV annihilation photon interactions in the scintillator modules on an event by event basis and use this information in the reconstruction algorithm. Otherwise for photons incident at oblique angles this would lead to parallax error resulting in generation of incorrect LORs contributing to the degradation of spatial reconstruction resolution. Following prior implementations described in the literature, we selected a dual sided readout PET module in which SiPMs are placed at both ends of a scintillation array and the ratio of the signal from one photodetector ($A$) divided by the sum signal of both detectors ($A+B$), as well as the $A$ vs $B$ plot are used to measure DOI.

### *B.1.2. PET panel imager*.

While the concept of the panel imager operating with the PET probe was described in the literature, to our

knowledge no prototypes have been built so far. The concept seems straightforward, and several types of panel modules could be built. There is no requirement for the panel module to be compact, for example it can be a sector from a standard PET scanner. However, compactness of the panel module offers advantages for example in the increased mobility of the dedicated PET system. In addition, in a special case, the panel can even serve as another insert into the PET/CT scanner. As discussed below in this submission, two modular technologies were chosen by us as candidates for the panel detectors: flat panel position sensitive PMTs, and Silicon Photomultipliers, SiPMs.

## C. Specific aims and corresponding milestones

From the instrumentation point of view, the goals of this project are: (1) design and develop a PET probe (based on previous prototypes) and produce two samples; (2) incorporation of one of the probes with the Siemens PET/CT scanner, (3) incorporation of the second probe with the panel PET imager in a dedicated prostate PET imaging system, (4) comparative studies of the PET/CT+probe and probe+panel systems against the same PET/CT but without probe, in realistic phantom studies.

From the biological markers point of view, the goals of this project are: (1) synthesis of new PET agents for PCa and (2) pilot tests of the dedicated probe+panel system using selected PET imaging agents for PCa.

To accomplish these goals, we have developed the following specific aims:

**Aim 1: Finalize design and build the endorectal PET probes with electronics (x2).**

• Milestone 1: Finalize probe design based on: (a) the latest (2011) developments in SiPM technology, (b) requirements from clinical end-users (oncologists/urologists), and (c) design specifications for read-out electronics and electronic interface with the Siemens PET/CT scanner.

• Milestone 2: Assemble the probe from prior selected and manufactured custom made scintillator arrays, SiPM arrays and read-out electronics.

• Milestone 3: Validate intrinsicPET probe performance in a stand-alone configuration (not connected to PET scanner and without combined image reconstruction).

Milestone 4: Manufacture the interface with the Siemens PET scanner and system test.

**Aim 2: Assemble and test the dedicated PET scanner: probe + panel**

• Milestone 1: Adapt the existing PEM/PET readout and trigger circuitry to the PET probe+PET panel system.

• Milestone 2: Adapt the existing PEM/PET reconstruction code to the PET probe+PET panel system, including the DOI information from the probe.

• Milestone 3: Measurements with phantoms.

**Aim 3: Design and develop reconstruction software for the probe+PET/CT scanner system.**

• Milestone 1: Identify most suitable reconstruction approach and algorithm.

• Milestone 2: Develop PET reconstruction code and test on Monte Carlo simulation.

• Milestone 3: Include CT information to assist with localization of the prostate and the probe.

• Milestone 4: Reconstruction of images of experimental phantoms.

**Aim 4: Perform pre-clinical phantom tests and measure the performances of the PET/CT scanner with the probe, and of the dedicated PET/probe imager**

• Milestone 1: Measure performance parameters (spatial resolution, count rate capability, sensitivity) of the PET/CT+probe

• Milestone 2: Measure performance parameters (spatial resolution, count rate capability, sensitivity) of the dedicated PET panel+probe system

• Milestone 3: Perform three-way comparison of the performances of the PET/CT+probe system, dedicated PET system and the conventional PET/CT scanner in realistic task-specific tests.

**Aim 5: Synthesis and radiosynthesis of new, mechanism-based PET agents for PCa, which can take advantage of this high-resolution imaging system.**

• Milestone 1: Radiochemical synthesis of up to ten new and one published PSMA-based PET imaging agents.

• Milestone 2: Preliminary animal imaging studies, to assure PCa uptake specificity, and dosimetry.

• Milestone 3: Development of Standard Operating Procedures (SOPs) and current Good Manufacturing Practice (cGMP) synthesis for human administration of the best of the newly synthesized compounds.

## D. Research strategy

### *D.1. Technology choice and plan of development*

Our research strategy in the instrumentation part of the prostate PET imager project relies heavily on recent relevant imaging technology developments at WVU and on our extensive experience in designing and building research PET imagers. What is most important, the proposed PET panel detector and PET probe modules will be prepared outside of and before the start of the project but will have to be adapted for the intended new system. We do not anticipate issues with this straightforward implementation of our well-established techniques for front-end electronics, DAQ, fast discrimination and trigger formation.
The important elements of this adaptation are the front-end readout system, and the data acquisition system accepting and digitizing signals from the readout system and then forwarding the digitized data to the computer system for data processing, data analysis and to tomographic image reconstruction.

### *D.1.1. Panel PET module*

For the initial panel detector in our demonstration project we propose to use the high performance PET imaging module employed before in the WVU breast PEM/PET imaging system (19,20). This high performance module has coverage of 20x15cm and is built based on a 4x3 array of H8500 flat panel PMTs, coupled to a matching size array of 2x2x15mm LYSO pixels. Reconstruction software developed by Smith (21,22) provided quick and accurate reconstruction of the scans. Excellent performance was obtained when using two pairs of these modules in the pilot breast imaging clinical trials (paper was submitted fro publication). Two of these modules (one pair) will be retired due to the upgrade of this high resolution dedicated breast scanner to a PET/CT variant. The CT component will take the place of the one PET pair. Readout electronics and data acquisition will be also provided with this panel imager. It is our plan, in a follow-up project, to replace this panel detector with an equivalent module made out of the SiPMs rather than PMTs. The compactess of SiPM will allow also to use this panel as another insert module inside the PET/CT scanner.

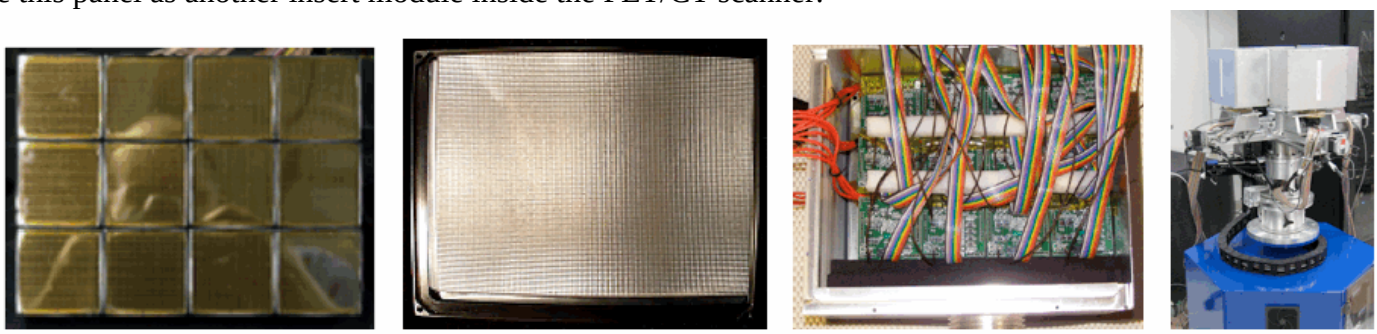

**Figure 5. The panel detector proposed for the stand alone prostate imager. This panel detector is built from an array of 12 (4x3) H8500 flat panel PMTs. An array of 2x2x15mm LYSO pixels spaced with 2.1mm pitch is coupled to the PMT array, forming a ~20x15cm imaging module. Two coincident pairs of these modules were successfully used recently in breast imaging clinical trials at WVU (20).**

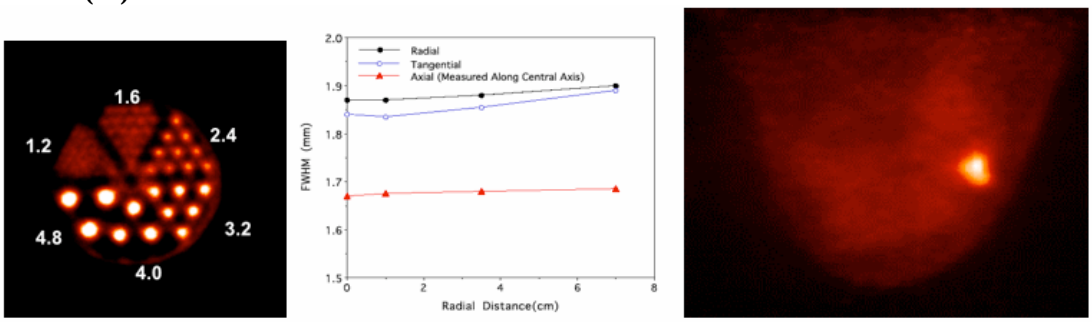


**Figure 6. Resolution of the PET system using two identical PET panel detectors, as proposed for this project, measured using phantoms, including the Derenzo phantom, at left. Right: Example of the patient breast image obtained with the system (20).**

The PET panel imager described above is equipped with 12 H8500 PMTs. Each PSPMT amplifier board provides four position-encoded analog signals and one analog sum signal for a total of 48 channels for the entire panel module (23,24). The analog sum of all PSPMTs in the detector is discriminated with a home-made constant-fraction discriminator (CFD). Similarly, the PET probe will be equipped with the resistive readout with

four position outputs, and a fast sum pulse then discriminated in a CFD discriminator for trigger purposes. Signal discrimination and event trigger are performed in the separate trigger hardware module (the same type as the one used in the WVU PEM/PET system).

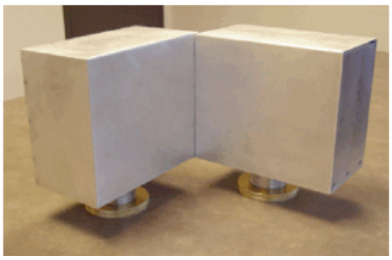

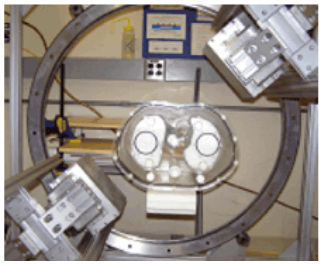

**Figure 7. The panel detector module will be attached to the computer controlled rotating gantry during phantom trials at WVU. This picture shows two of the same modules before and after being attached to the gantry, during an experiment demonstrating the dedicated PET scanning system composed of two panel imagers.**

In the next step of development (beyond the scope of the present submission) we will develop the replacement module for the PMT based panel detector, based on SiPM technology. We embarked on this development under a different grant, and if time permits on a time scale of this project we may want to try this replacement. The interesting element of this development is that the fure SiPM based panel module can be interpreted as another insert in the PET/CT scanner.

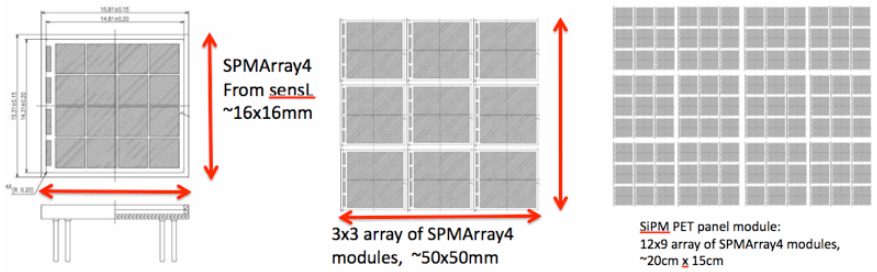


**Figure 8. The proposed next generation 20cm x 15cm prototype panel photodetector concept is based on an array of 108 SPMArray4 modules arranged in a 12x9 array. Each SPMArray4 module shown at left is made out of 16 ~3x3mm SiPM units. The panel detector will be built from an array of 4x3 ~5cm modules, and each of these modules will be made of an array of 9 SPMArray4 modules. This panel module will be used to substitute the previously described PMT based photodetector, while the scintillator array will be the same.**

### *D.1.2. PET probes*

We have selected SiPM technology for the endorectal prostate PET probe. The SiPM technology is compact, utilizes much lower voltage than APDs (clinical safety of use), and has high S/N, allowing for constructing very compact systems with minimal electronics on board of the probe. The SiPM probes are very compact and can be also implemented as inserts to MRI with minimal interference with MRI imaging quality. The published literature on the SiPM based biomedical imagers is growing dramatically in the last few years due to increased availability of commercially available SiPMs and increasing reliability, while costs are decreasing. Many of these papers focus on the MRI compatibility of the SiPMs (our own presented unpublished results have shown that even at 14 Tesla affects are small) and on design and construction of the PET inserts to be used inside MRIs (a good examples is this effort are: (25,26,27). A very related effort is the one by the Korean group, using the same type of sensL SiPM modules used by us in the prostate probe prototypes, but in the brain imager (28,29,30). Other group of relevant papers is describing the devices based on MPPC sensors from Hamamatsu (31) and (18).

The only disadvantage of SiPMs (beyond their still high costs) is their temperature sensitivity. However, this can be corrected by constantly monitoring the temperature of the probe with a miniature on board temperature sensor We have built several operational prototypes of the SiPM probes, some explicitly intended for prostate, and we will use the latest designs for our endorectal PET probes for the two imaging systems. Fast readout electronics and DAQ used in the WVU PET/PEM system will be adapted for the dedicated PET panel+probe imager. Also, the prototype read-out will be adapted to be compatible with the Siemens PET/CT. Section D2 of in this document will be fully dedicated to the description of our present generation of SiPM probes, a key element of the proposal. Another sensor on the probe will be a microBird positioner allowing tracking the position of the probe relative to the reference system.

The probes with the affiliated gear, mechanics, on-board sensors (position, temperature) and readout will be provided through additional funds and will be not charged to this grant.

### *D.1.3. DAQ for the prostate PET panel and the PET probe.*

Our selected well-tested solution for the high performance data acquisition system of the stand-alone prostate PET imager is the FPGA-based USB data acquisition system designed and developed originally at Jefferson Lab. We have successfully implemented and validated such a system in the PEM/PET imager at WVU validated recently in clinical trials (20). This system has a modular, extensible architecture with up to 64 channels of simultaneous-sampling ADCs per unit and a sustained trigger rate of over 150 kHz for all 64 channels (32,33). In standard operation, each unit corresponds to one individual detector module. Each coincident pair of modules is time synchronized in order to match event timing of the two detectors. Both corresponding units are triggered simultaneously by the external coincidence trigger logic. Each DAQ unit sends time-stamped raw event data over high-speed USB to its own acquisition computer. Each acquisition computer performs then centroid and energy calculations on all incoming data and sends this time-stamped processed data over gigabit Ethernet to the event builder/reconstruction computer (34). The event builder uses the time stamps to merge the separate detector events into a single coincident event. It may also perform image reconstruction or send the data to another computer for image reconstruction. The set of reconstructed tomographic images is sent to a user interface. In the operational mode with the endorectal probe, the data events from the probe are recorded in its own DAQ module in coincidence with the panel PET imaging module, and like all the other data is recorded with a time stamp.

**Figure 9. Fast FPGA-based multi-channel DAQ electronics circuitry developed by James Proffitt (now at AiT). One 64 channel system like this would read all the channels of the dedicated prostate PET system (panel+probe).**

### *D.1.4. Readout for the PET/CT scanner with the prostate PET probe*

There are two key technical issues to resolve when operating the prostate PET probe with the PET/CT scanner and they both require close collaboration with the PET/CT technical team (from Siemens in this case): (1) electronic readout and trigger, (2) software reconstruction algorithm. The first issue will be resolved by matching the readout output of the prostate PET probe to the inputs provided on the PET scanner. We will use resistive readout that was already proven by several prior art efforts. Two x 4 Anger logic type outputs (from both sides of the DOI scintillation module) coming from the PET probe will be connected to the extra inputs on the PET/CT scanner. The WVU/UM/Siemens team will work on the reconstruction algorithm of the PET+probe system.

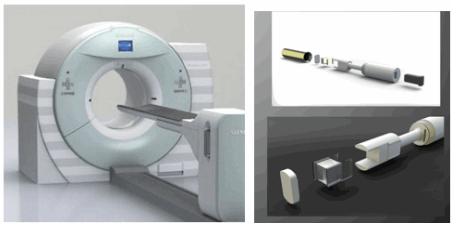

**Figure 10. Picture of the Siemens PET/CT scanner, and the concept of the endorectal PET probe, shield.**

### *D.1.5. Reconstruction approach*

The coincidence data will be acquired in list mode and image reconstruction will be performed using a three dimensional, maximum likelihood expectation maximization (3D-MLEM) algorithm. A statistical iterative algorithm of this type is ideal for our unique imaging geometries of 1) an endorectal PET probe with an external conventional PET detector ring and 2) an endorectal PET probe with a PET panel detector. 3-D MLEM algorithms can handle non-standard positioning of the detectors and lines of response (LORs) for the forward and backprojection steps of the algorithm. Incorporation of the point spread function (modeled or simulated) and time of flight (TOF) information, if available, will be considered. We will evaluate options for reconstructing the data directly from the list mode data and also from events rebinned into sinograms. Particular attention will be dedicated to techniques to properly correct the data during image reconstruction, namely randoms, normalization, attenuation and scatter corrections.

The input list mode data for case 1) of a probe interfaced to a PET/CT scanner typically will include, for each event in the coincidence pair: the block ID (either in the ring or in the probe), crystal or XY ID in the

block, depth of interaction (DOI) or Z ID in the crystal, time-of-flight difference for the coincidence pair, and prompt or random coincidence tag. For case 2) of a probe and a PET panel detector, the list mode data for each event will include the block ID of the probe, the XY ID in the block, the crystal identifier in the flat panel detector, and DOI and TOF timing information if available.

Key information needed for the 3D-MLEM algorithm for both the probe-ring and probe-panel geometries is the spatial position of the endorectal PET probe with respect to the external PET detector, which will be patient-dependent. Several options will be considered to determine such information. The location and orientation of the endorectal detector will be monitored using a compact positioning system that we have used previously. Specifically, we plan to utilize the micro-Bird™ system from Ascension Technologies, Inc., which is comprised of a small transmitting unit (attached to the detector unit) and an external receiver. If our goal of maintaining a constant orientation between the endorectal and external detectors is not possible based on the acquired position data, the time-stamped list-mode coincidence data will be used together with time-stamped endorectal probe position information in a unified list-mode image reconstruction algorithm modeling motion between the endorectal probe and the external detector ring or panel.

The implementation of the MLEM algorithm will be adapted from a previously developed version designed for positron emission mammography (PEM) imaging (21) and optimized for very rapid reconstruction of images on a multi-processor computer (22). We will investigate strategies such as data partitioning to accelerate image reconstruction. Rapid image creation is important if we are to use the images to guide biopsies (including needle position verification) without significantly lengthening the procedure time.

***D.2. Initial SiPM probe studies.*** The PET probe will be built based on the SiPM technology. We tested the first samples of the SiPM imaging modules based on MPPC units from Hamamatsu and from SensL. The pilot test results are shown below. Our standard multichannel FPGA DAQ system (32, 33) was used to collect the data and Kmax toolsheet on a PC (34) to analyze the data. Several sizes and shapes (also round) of MPPC based arrays were tested also for application in hand-held surgical imagers.

**Figure 11. Left: First prototype of a compact full size (3cm wide by 2cm tall) endorectal prostate PET probe (without DOI capability). At left is the photodetector sensor area built out of 72 MPPCs arranged in a 6x12 array. The 3x3xmm MPPC units were spaced at 5mm center to center distance. In the center is the input stage electronics (amplifiers) and at right is the bank of cable connectors matching with three small profile flat cables. Side view of the probe with a 1cm thick LYSO array shows how compact indeed is the design of this SiPM array prototype. The thickness of the total assembly is practically defined by the combined radiation sensor (scintillator) and the light guide. Center: Three key components of the PET probe. Light spreader window provides light sharing between individual MPPC units in the array. Light sharing has to be efficient enough to bridge the dead regions between the MPPC units. LYSO array of 1.5x1.5x10mm pixels (from Proteus). Right: Raw image obtained with the LYSO array coupled to the MPPC array.**

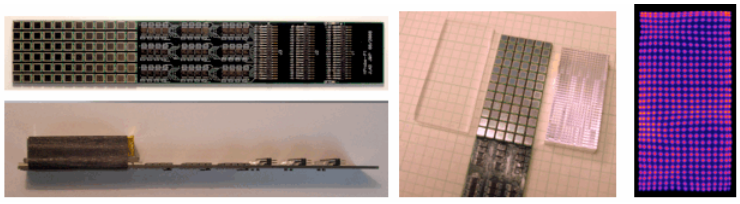

**Figure 12. Other type of MPPC based modules tested. Left: an array of 25 (5x5) MPPCs spaced at 5mm to c over the area of ~1" square. Center: the photodetector board with an array of 80 Hamamatsu 3mm MPPCs, spaced at 6mm, center-to-center. The round array had cables exiting to the side to minimize its thickness for a hand-held operation.**

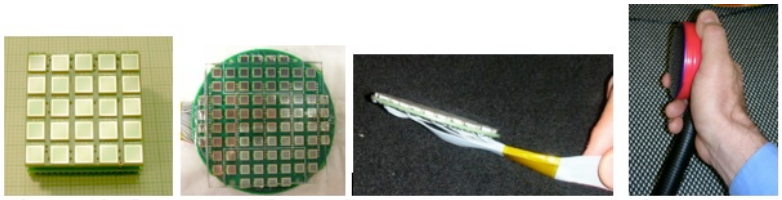

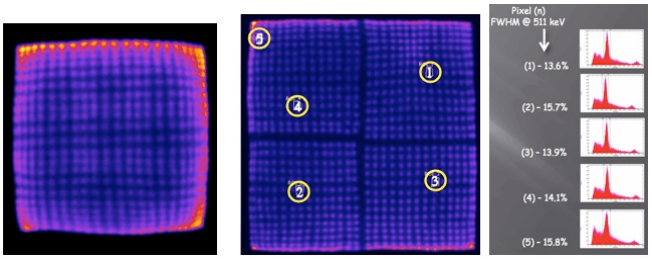


**Figure 13. Left: Raw image of 1x1x10mm LYSO pixel array obtained on the 1" 25ch MPPC module. Raw image at center shows good separation of the 1.5mm LYSO pixels in the round array. Five LYSO pixels were selected for energy histogram measurements. (The four sectors seen in the image are due to four separate sub-arrays used to cover the FOV of the imager.) Despite surface coverage of only ~25% excellent energy resolution (13.5-16% FWHM@511 keV) was obtained.**

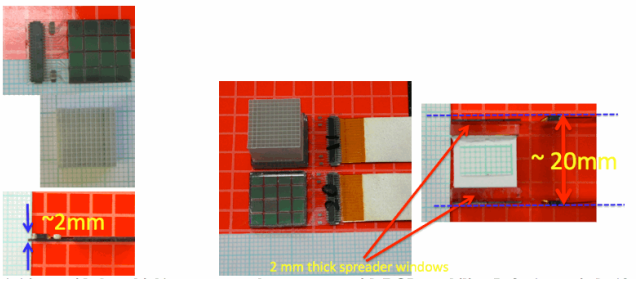


**Figure 14. Second, small size (~14mm wide by ~ high) prostate probe prototype with DOI capability. Left: 1mm pitch, 10mm thick 12x12 pixel LYSO scintillator array from Proteus, with 50 micron Lumirror septa for DOI operation, coupled to the very low profile (<2mm thick) sensL 16ch SPMArray2 module, shown from the top and in a side view. Right: 1mm DOI module during assembly with two SiPM modules coupled at both sides of the LYSO array. Glass 2mm thick spreader windows are inserted between the arrays and SiPM modules. Sylgard 3-6636 silicone gel was used as optical coupling between all optical surfaces.**

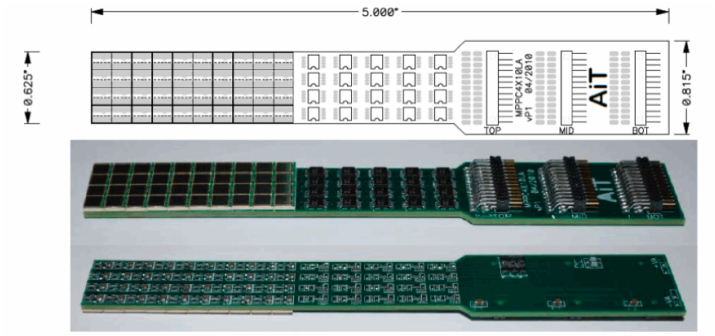


**Figure 15. New prototype (May 2010) of the PET probe built by AIT with ~ 15mm x 45mm active FOV. The photosensor part is made out of a 4x10 array of Hamamatsu MPPCs. Two of these units will read light from two sides of the DOI scintillation array.**

### *D.2.1. Preliminary studies of the DOI prostate probe prototype.*

Our experimental apparatus consisted of a 12x12 scintillation array with 1x1x10 $mm^3$ pixels (Proteus) with 50 micron Lumirror septa for DOI optimization. The scintillator was optically coupled (Stylgard 3-6636 silicon gel) to two low profile (~1mm thick) 4x4 element SiPMs with 3 x $3mm^3$ pixels (SPMArray2 from sensL). A 12x12x2mm AR coated UV fused silica light spreader window (Edmund Optics) was placed between both SiPM/scintillator interfaces. FPC cables were used to interface the PET module to custom 16 channel differential pre-amplifiers connected to evaluation/power supply boards (SPMArray2-A0 and SPMArray2-A1 respectively from sensL). Data was acquired via a FPGA-based USB system which has a modular extensible architecture with up to 64 channels of simultaneous sampling ADCs per unit, and a sustained trigger rate of over 150kHz for all channels (32,33). A custom designed Kmax toolsheet (Sparrow Corp.) was used to analyze the data (34).

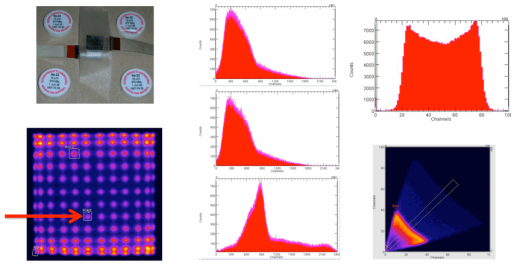

**Figure 16. Results obtained with the 1mm DOI module and a broad 511 keV beam from four $^{22}Na$ sources. Bottom-left: uncorrected raw image obtained with one of the SiPM modules. All 144 LYSO pixels are visible. One 1x1x10 $mm^3$ LYSO pixel was selected for these studies. Center: energy spectra for the selected LYSO pixel: Output 1 (top), Output 2 (center), Sum (bottom). Top-right: Output 1-to-Sum signal ratio histogram (horizontal scale is in percent). Right-bottom: Output 1 vs Output 2 plot.**

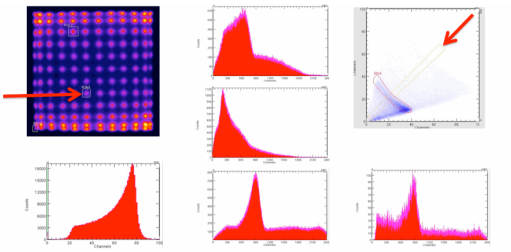

**Figure 17. Results obtained with the 1mm DOI module and a $^{22}Na$ 511 keV beam entering the module from the Output 1 (top) side. One central 1x1x10 $mm^3$ LYSO pixel selected. Left-top: uncorrected raw image obtained with Output 1 SiPM module. Left-bottom: Output 1 versus Sum (Output 1 + Output 2) histogram (horizontal scale in percent). Center: energy spectra for the selected LYSO pixel: Output 1 (top), Output 2 (center), Sum (bottom). Right-top: Output 1 vs Output 2 plot. Right-bottom: Sum output for the selected ROI region in the top plot (selecting ~DOI center region of the pixel).**

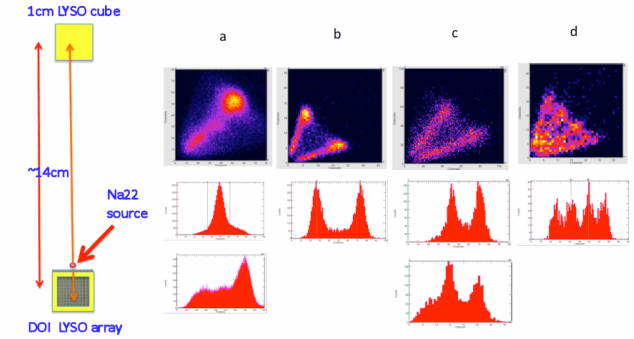


**Figure 18. Several measurements of the DOI resolution using Na22 sources and capillaries filled with F18 solution. Electronically collimated beams of 511 keV annihilation rays were produced by using a 1 cm cube LaBr3 crystal mounted to a small PMT as a coincident detector with the 1mm LYSO array, as shown at left. Column a: single 1mm diameter source, b: two Na22 sources placed at 6.5mm, c: two capillaries at 5mm, d: four capillaries at 2.5mm. At top are shown plots of scintillation signals measured for a single LYSO pixel in one SiPM array versus the other (output 1**

**vs output 2). In the central section are histograms of output 1 vs sum of the two outputs. At bottom are shown energy spectra. Energy spectrum at left is the sum of both outputs for the selected single LYSO pixel. Energy spectrum at right is output 1 for the two-capillary case, showing energy variation with DOI.**

While prior publications indicate nearly linear DOI spatial resolution of ~2 mm is attainable (35) for such a design, we were able to demonstrate that PET modules with DOI spatial resolution ~1.5mm FWHM are indeed possible using specially prepared 1mm LYSO arrays. This improvement in DOI spatial resolution will result in further reduction of parallax error, therefore enhancing the quantitative accuracy of reconstructed images (36). For limited parallax errors expected in realistic PET systems, and when combined with ~1mm resolution in the scintillator plane, the obtained result indicates that ~1mm resolution PET imaging is possible with the selected technical approach.

### *D.2.2. Relevant studies of the SiPM panel imager prototypes.*

While we are not proposing to implement this technology in the PET panel detector in this project, but we are very actively working on detector modules based on Hamamatsu MPPCs and sensL SPMArrays4 for other projects. Several detector modules of square, rectangular and round shapes (for surgical imaging applications) based on MPPCs were constructed, however their coverage is up to ~5cm only. Working with sensL, new planned modules (but not yet available) will be of ~5x5cm active FOV and will be tileable to be able to cover larger FO, such as 15x20 cm, and at economical cost, comparable to the cost of flat panel H8500 PSPMTs.
We have tested briefly the 4x4 array of SPMArray4 modules made available for our evaluation from sensL. The system performed well and an example of the energy spectrum from a 3x3x15mm LYSO pixel coupled to one 3mm sensor from one SPMArray4 modules is shown in the figure below.

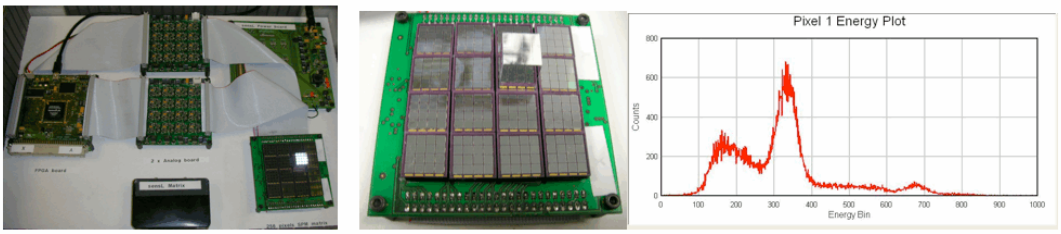


**Figure 19. Prototype SPMArray4 system of 256 3mm SiPM pixels with electronics and FPGA DAQ readout from sensL. During the initial laboratory tests (May 2010) a matching 4x4 LYSO pixel array was coupled to one of 16ch SPMArray4 modules, and the example of the obtained energy spectrum with a Na22 source is shown at right. Two gamma peaks of 511 keV (annihilation photons) and 1274 keV (gammas) can be distinguished.**

### *D.3 Description of the Approach, Milestones, and Timeplan (in SOW -Attachment 5).*

### *D.4. Rationale and preliminary studies – imaging agent development.*

In addition to the unpublished work discussed below, we have published several previous papers and a review describing our PSMA-based imaging agents (37), (38), (39), (40), (3), (41), (42), (43), (44), (45), (46). We have also generated several patents and patent applications based on this work, all of which have been licensed (to BIND Biosciences, Principio and Molecular Insight Pharmaceuticals). Abstracts presented at the 2007 (and soon at the 2010) SNM meeting that described a urea-based PSMA imaging agent for SPECT received the Berson-Yalow award (47). That work was performed by Molecular Insight Pharmaceuticals in collaboration with our laboratory. Initially we synthesized radiolabeled analogs of urea-based PSMA inhibitors previously described by Kozikowski et al (35), (36),(39). Those compounds have become to be known as *N*-[*N*-[(*S*)-1,3-dicarboxypropyl]carbamoyl]-*S*- [$^{11}$C]methyl-L-cysteine, [$^{11}$C]DCMC ($K_i$, 3.1 nM), *N*-[*N*-[(*S*)-1,3-

Scheme D.1


**Figure 20**

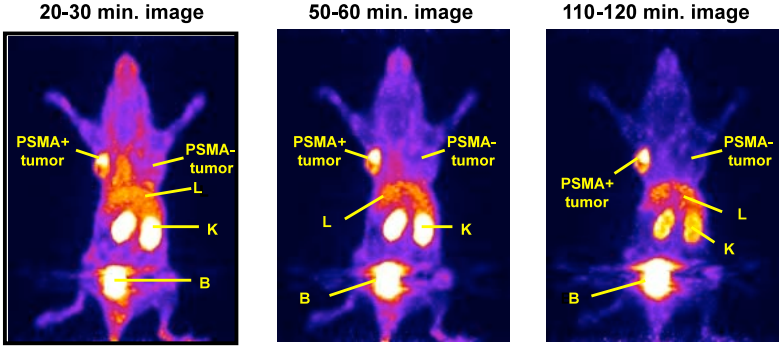

dicarboxypropyl]carbamoyl]-*S*-3-[$^{125}$I]iodo-L-tyrosine, [$^{125}$I]DCIT ($K_i$, 1.5 nM) and *N*-[*N*-[(*S*)-1,3-dicarboxypropyl]carbamoyl]-4-[$^{18}$F]fluorobenzyl-L-cysteine, [$^{18}$F]DCFBC (**Scheme D.1**). Those compounds were designed and prepared prior to publication of the crystal structure of PSMA. Imaging data provided by them has been encouraging, with [$^{11}$C]DCMC demonstrating an 11:1 tumor (LNCaP) to muscle ratio at 30 min post-injection and [$^{125}$I]DCIT showing a 5:1 ratio. By the time we synthesized [$^{18}$F]DCFBC, we used a more specific model to study binding selectivity, i.e., tumors derived from what are normally PSMA-negative PC-3 PCa cells vs. those derived from PC-3 cells engineered to express PSMA (courtesy of Dr. Warren Heston). [$^{18}$F]DCFBC demonstrated a 20:1 target to nontarget ratio at 2 h post-injection, at which time it was concentrated in tumor to a level of 5% injected dose/gram (**Figure 20**). Notably, the engineered PC-3 tumors express much less PSMA than LNCaP tumors, but we believe the comparison of PC-3 PIP (PSMA+) vs. PC-3 FLU (PSMA-) to be more valid than PC-3 vs. LNCaP, which demonstrate different degrees of vascularity.

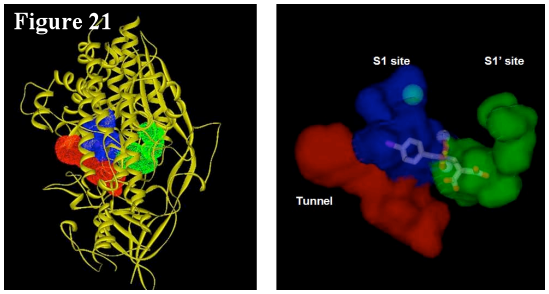


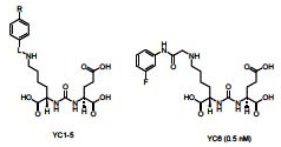

Table D.1. YC halogen series of lys-urea-glu

| No | L | R | $IC_{50}$ (nM) | Radiolabelling |
|---|---|---|---|---|
| YC1 | -C(=O)- | F | 0.3 | - |
| YC2 | -C(=O)- | I | 0.06 | $^{125}$I |
| YC3 | -$CH_2$- | F | 15 | - |
| YC4 | -C(=O)$CH_2$ON=CH- | F | 0.4 | $^{18}$F |
| YC5 | -C(=O)- | $C_6H_4F$ | 0.04 | - |

More recently we have begun employing the high-resolution crystal structure of PSMA to design agents for SPECT as well as PET-based agents that may have superior pharmacokinetics (42). (We do not know how [$^{18}$F]DCFBC will perform in human subjects.) **Figure 21** uses the DS ViewerPro software (Accelrys Inc.) to demonstrate the active site of PSMA with GPI-18431 (PDB ID: 2C6C) (48). Two substrate binding sites (S1': glutamate-binding pocket, S1: amphiphilic binding pocket) comprise the active site of the enzyme. A tunnel-like region linked to the S1 binding pocket is projected toward the surface of the enzyme, and tolerates considerable bulk. We have found that glutamate must remain essentially invariant within the S1' binding pocket. Accordingly, all of our inhibitors to date have had a terminal, "eastern" glutamate. The "western" lysine was fitted in the S1 binding site and was found to be able to replace serine and tyrosine shown in DCMC, DCFBC, and DCIT. We have synthesized PSMA inhibitors with Lys-urea-Glu as a core scaffold.

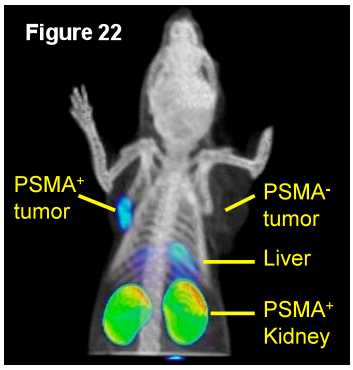


In the first approach, we utilized the amphiphilic S1 binding site and synthesized six Lys-urea-Glu analogs. Their chemical structures and *in vitro* $IC_{50}$s are summarized in **Table D.1**. *In vitro* NAALADase assay showed that all of these compounds were more potent than the original compounds of Kozikowski et al. Using a newly constructed hot cell in our laboratory, YC2 and YC4 were radiolabeled with $^{125}$I and $^{18}$F, respectively. Compound YC2 was synthesized *via* radioiododestannylation in 65-80% radiochemical yield at specific activities ranging from 1,000 to 1,300 Ci/mmol. Compound YC2 provided the image in **Figure 22** at 4 hrs post-injection. Compound YC4 was synthesized from [$^{18}$F]fluorobenzaldehyde in 30% radiochemical yield and specific radioactivity of 1,500 Ci/mmol.

**Figure 23**

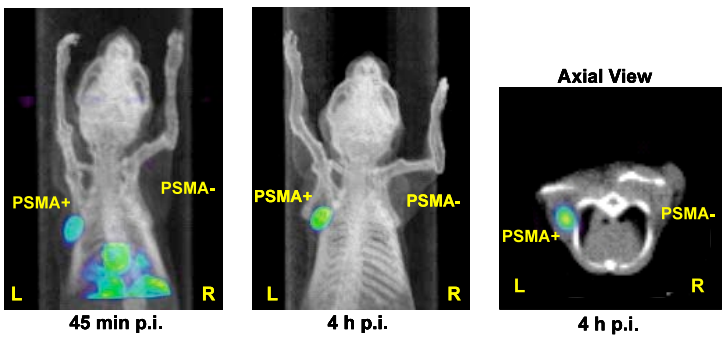


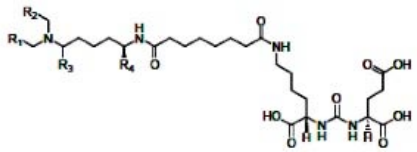

Table D.2. L series of Re and 99mTc-labeled compounds

| No | R1 | R2 | R3 | R4 | Metal | $IC_{50}$ (nM) | Radiolabeling |
|---|---|---|---|---|---|---|---|
| L1 | 2-pyridine | 2-pyridine | H | $CO_2H$ | -/Re | 8.5/14.2 | $^{99m}$Tc |
| L2 | 2-quinoline | 2-quinoline | H | $CO_2H$ | -/Re | 0.2/0.6 | $^{99m}$Tc |
| L3 | 2-pyridine | 2-pyridine | $CO_2H$ | H | -/Re | 2.2/13.9 | $^{99m}$Tc |
| L5 | 2-pyridine | $CO_2H$ | H | $CO_2H$ | -/Re | 1.6/0.7 | $^{99m}$Tc |
| L4 | 2-pyridine | $CO_2H$ | H | H | -/Re | -/1.6 | $^{99m}$Tc |

In the second approach, we utilized the tunnel region in the vicinity of the S1 binding site,

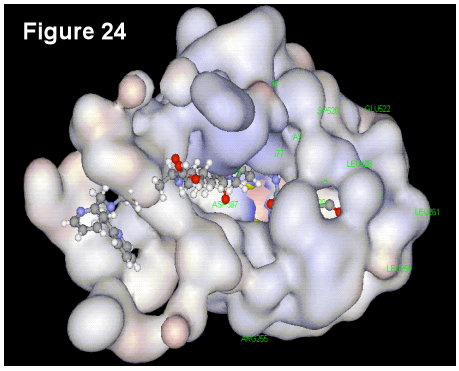


which is approximately 8 x 8 x 20Å in space. We hypothesized that the linker length between the bulky metal-coordinating group and the urea should be longer than 20Å. Analogs **L1-5** (**Table D.2**) have a spacer length of > 20Å and demonstrated suitable inhibitory capacity *in vitro* as well as having provided clear tumor delineation *in vivo*, with little background at 4 h post-injection (**Figure 23**) (41). PIP:FLU ratios of over 40:1 were achieved within 2 hrs post-injection. Radiochemical yields are on the order of 70-80%. Figure 12 shows binding of **L1** (**Table D.2**) to PSMA with the glutamate portion of the molecule within the S1' binding pocket (DS ViewerPro 6.0 software). It is upon the **L1** scaffold that we are basing the new ligands to be synthesized for this proposal.

We have determined PSMA crystal structures with our urea-based PSMA imaging agents including DCMC, DCFBC, DCIT, and YC2. As shown in **Figure 25** and in (42), all of our compounds (DCIT not shown) bind to the active site of PSMA in a similar binding mode. The glutamate portion binds to the S1' pocket without any change in 3D space, i.e., its position is invariant between the compounds tested, while substituents in the S1 pocket showed a certain degree of flexibility. One key feature of our urea analogs is the strong interaction between the carboxylic acid In the second approach, we utilized the tunnel region in the vicinity of the S1 binding site, which is approximately 8 x 8 x 20Å in space. We hypothesized that the linker length between the bulky metal-coordinating group and the urea should be longer than 20Å. Analogs **L1-5** (**Table D.2**) have a spacer length of > 20Å and demonstrated suitable inhibitory capacity *in vitro* as well as having provided clear tumor delineation *in vivo*, with little background at 4 h post-injection (**Figure 23**) (41). PIP:FLU ratios of over 40:1 were achieved within 2 hrs post-injection. These compounds were prepared by Dr. Sangeeta Ray Banerjee, who developed the corresponding chelation technique, i.e., the single amino acid chelator (SAAC) concept, during her postdoctoral studies at Syracuse University (49), (50), (51), (52), (53). Radiochemical yields are on the order of 70-80%. **Figure 24** shows binding of **L1** (**Table D.2**) to PSMA with the glutamate portion of the molecule within the S1' binding pocket (DS ViewerPro 6.0 software). It is upon the **L1** scaffold that we are basing the new ligands to be synthesized for this proposal.

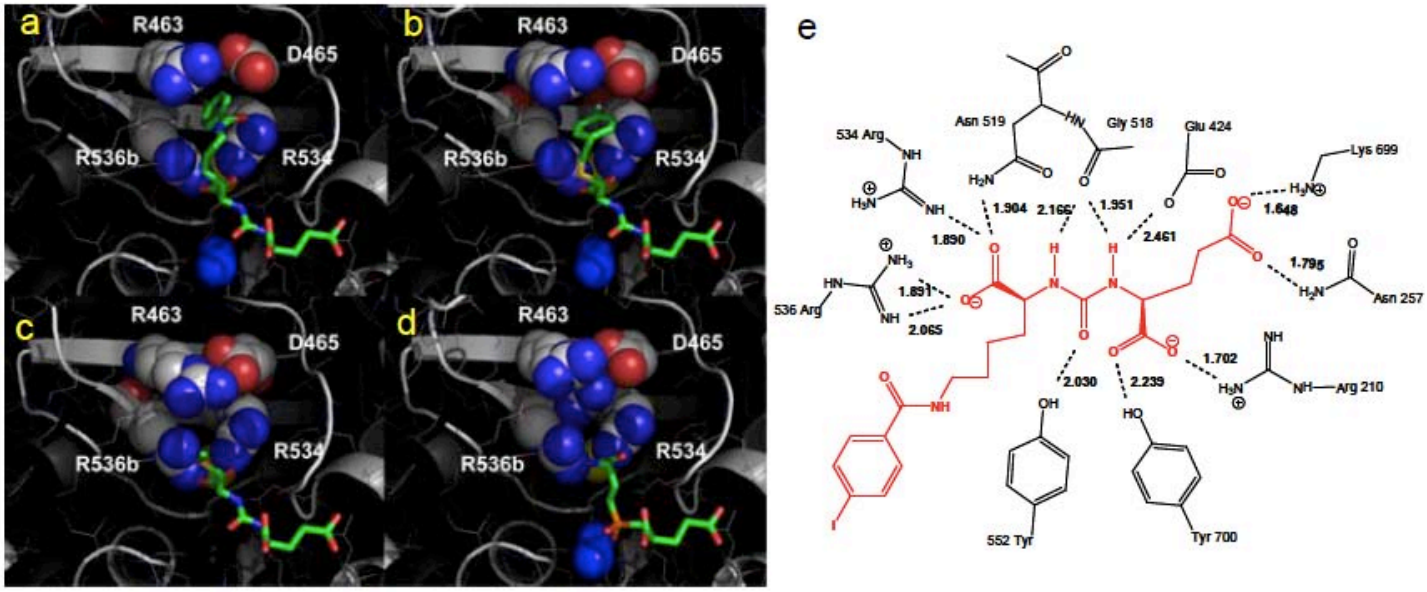


**Figure 25. (a) PSMA with YC2, (b) PSMA with DCFBC, (c) PSMA with DCMC, (d) PSMA with the phosphite analog, GPI-19806 (e) 2-D schematic representation of YC2 in the active site of PSMA.**

We have determined PSMA crystal structures with our urea-based PSMA imaging agents including DCMC, DCFBC, DCIT, and YC2. As shown in **Figure 25** and in (42), all of our compounds (DCIT not shown) bind to the active site of PSMA in a similar binding mode. The glutamate portion binds to the S1' pocket without any change in 3D space, i.e., its position is invariant between the compounds tested, while substituents in the S1 pocket showed a certain degree of flexibility. One key feature of our urea analogs is the

strong interaction between the carboxylic acid in the *N*-terminal region and the "arginine patch" of the S1 pocket, which includes Arg 534 and 536 (**Figure 25e**). This may explain why urea-based PSMA imaging agents demonstrate PSMA inhibitory activities in the nanomolar range despite a variety of modifications on moieties that project into the S1 pocket.

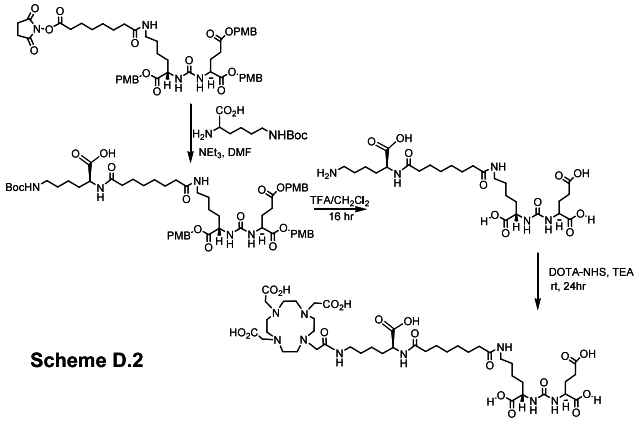


**Scheme D.2**

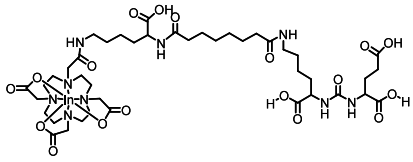

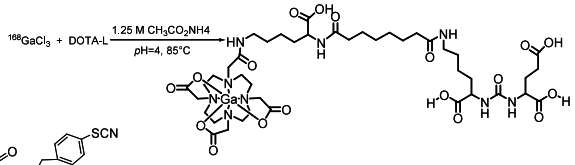


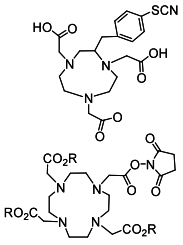

**Scheme D.3**



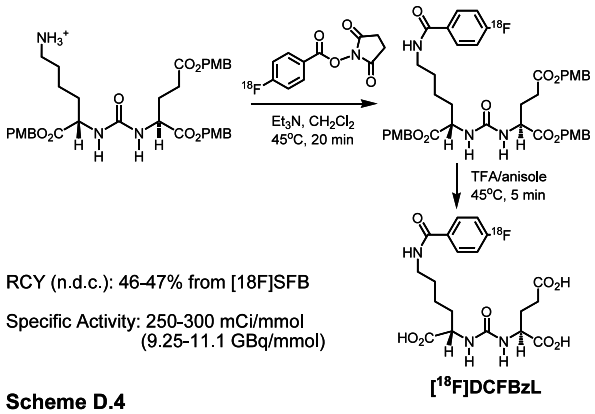


**Scheme D.4**

***D.5.1 Realization of aims relevant to imaging agent development: methods.*** Compound [$^{68}$Ga]**L1** is based on our highly successful metalated SPECT series discussed above, however we will replace the $^{99m}$Tc-DMP with $^{68}$Ga and a suitable chelator. The rationale for this is two-fold, 1) to transform our best SPECT agent into one for PET and 2) to utilize $^{68}$Ga, which is increasingly recognized as a premier PET imaging nuclide (physical half-life = 68 min), particularly for tagging low molecular weight agents with relatively rapid pharmacokinetics, as is the case with our proposed compounds. The synthesis of [$^{68}$Ga]**L1** is shown in **Scheme D.2**. Use of an alternative chelator is shown in **Scheme D.3**, which may provide different pharmacokinetics and stability than the standard DOTA chelator (54). All synthetic steps are standard, and previously performed by us (41). Once the radiochemical synthesis is optimized, we will perform an *in vitro* PSMA binding assay (the NAALADase assay) to assure high affinity for PSMA, as well as *ex vivo* biodistribution and *in vivo* rodent (imaging) studies, all using methods previously published by us (38), (55), (3). We will also apply to the NCI Experimental Therapeutics (NExT) Program for toxicity evaluation and develop standard operating procedures (SOPs) for the synthesis of [$^{68}$Ga]**L1** according to GMP, as we have done previously for other radiopharmaceuticals we have administered to human subjects. We have had at least three previous compounds that obtained their toxicity data courtesy of the NIH.

Compound [$^{18}$F]DCFBzL (**Scheme D.4**) has undergone preliminary imaging and *ex vivo* biodistribution studies that demonstrate highly selective binding to PSMA+ PIP tumors, with significant tumor uptake (8.58 ± 3.09 % ID/g at 30 min p.i.). As such we envision this as a next-in-line PSMA-based PET imaging agent, behind our first-generation compound, [$^{18}$F]DCFBC, discussed below. [$^{18}$F]DCFBzL demonstrates higher overall binding to PSMA+ tumors than [$^{18}$F]DCFBC, and it displays > 20:1 target:nontarget ratios at one hour after injection. Its synthesis is shown in **Scheme D.4**, all using standard chemical transformations. We will also apply to NExT for toxicity studies and develop SOPs for GMP synthesis of this compound. Because of our familiarity in the synthesis and radiosynthesis of this class of compounds, as well as our ability to manipulate the pharmacokinetics of these compounds through alterations in the linker between the PSMA-binding moiety (urea) and the chelator, we also intend to synthesize the six agents shown in **Scheme D.5**. Our excitement about pursuing the $^{18}$F-labeled compounds in that series is based on recent work by McBride et al. in which $^{18}$F can now be introduced to a wide variety of biomolecules through an aluminum chelate *via* NOTA conjugation (56).

We have already synthesized several NOTA analogs of our PSMA-binding ureas and are eager to apply them to the development of pharmacokinetically optimized compounds. These syntheses, although related to that of [$^{68}$Ga]**L1**, will be undertaken as backup to the aforementioned targets. Their toxicity studies and synthesis according to cGMP are beyond the scope of this proposal.
[$^{18}$F]DCFBC has already undergone toxicity testing (courtesy of the DCIDE – a precursor of the NExT program – program at the NCI) and has been shown to be nontoxic. Dosimetry studies also demonstrate no significant concern, with kidney as the target organ. We have applied to the FDA for human testing. This will be the first of the new compounds that we intend to test in the first clinical trials following this project.

***D.5. Statistical considerations.*** For *ex vivo* biodistribution assays (Aim 5), four animals per time point at six time points per study has been the standard for demonstrating significance, i.e., higher radiopharmaceutical uptake in PSMA+ vs. PSMA- tumors, for compounds of this class. We estimate using a total of 96 SCID mice in this proposal (four *ex vivo* biodistribution assays). We need not perform *ex vivo* (biodistribution) assays on all compounds synthesized as we will be able to image them all as an initial screen. Only those with passable pharamacokinetics, namely $\geq$ 3:1 PSMA+ to PSMA- tumor uptake ratio, will go on to fully quantitative biodistribution. We can also use the same mice for imaging prior to *ex vivo* biodistribution.

**E. Project coordination**

While having only two leading PIs (Dr Pomper and Dr Majewski), our team will be composed of four entities: Johns Hopkins University group (led by Dr. Martin Pomper), West Virginia University group (led by Dr. Stan Majewski), Siemens Healthcare Molecular Imaging group (led by Dr. Maurizio Conti), the University of Maryland member (Dr. Mark Smith), and a consultant, Dr Yuan-Chuan Tai, from Washington University in Saint Louis, an inventor of the PET magnification concept. The West Virginia University partner will be responsible for all the instrumentation part. It will develop two endorectal PET probes and the PET panel detector. With assistance from UM and Siemens there will be two systems prepared: one PET probe will be connected to and tested with the Siemens PET/CT scanner, and the second probe and the panel imager will be prepared as the stand-alone prostate PET imaging system. The reconstruction software for the PET/CT+probe system will come from the close collaboration between Dr Conti and Dr Smith, with advise from Dr Tai. Siemens Healthcare Molecular Imaging will develop an interface of the probe to the present generation of Siemens PET/CT scanners, a joint expanded WVU/UM-Siemens group will develop reconstruction software. The algorithm for the dedicated PET system will be developed by Dr Smith, who will supervise a post-doc at WVU. The post-doc will assist with both reconstruction software tasks. The comparative task-specific performance of the two systems against the standard PET/CT scanner without probe, will be performed in the laboratory setting at the Siemens Healthcare Molecular Imaging site, using realistic phantoms. Through the duration of the project, Dr. Pomper will have complete responsibility for the imaging agent development side of the project. He will inform other partners of the scientific progress related to the project goals.
The second system (Siemens PET/CT + PET probe) will be validated and tested with phantoms, and it will be ready for pilot patient studies, but in the next following project, when more funds will be available to cover the cost of the hybrid system rental or adaptation of the existing Siemens scanner. From this plan, it is obvious that the preclinical validation tests, first at WVU and then at Siemens, will require the closest coordination of effort, between the WVU/UM group with the Siemens group.
Most of the team members know each other well from the past common work. For many years until 2009 Dr Majewski led the Detector and Imaging group at Jlab and his group had extensive ongoing collaborative effort with the group of Dr. Pomper and his collaborators in the Small Animal Imaging Resource Programa at JHU. This collaboration was dating back over eight years, providing therefore a firm basis for the new project PI cooperation. Another ex-Jlab team member, Dr Alexander Stolin, who participated in the Jlab-JHU collaboration in the last couple of years, also joined few months ago the WVU group and will take part in this effort. Dr Smith who is a well-known expert in PET reconstruction software, was a member of the Jlab group when Dr Majewski was the group leader there, and is now collaborating on two projects with WVU (with Dr Raylman as a PI). Dr Pomper also knows well Dr. Smith from his work on the Jlab/UM/JHU projects. Dr. Conti is a leading scientist at Siemens Healthcare Molecular Imaging for the development of new PET architectures and systems, and was instrumental in the development of the new generation of TOFPET

scanners. The two PIs (Dr Pomper and Dr Majewski) got to know Dr Conti during the last year, and they all share the same strong motivation to assist with the task of better prostate cancer detections and treatment. Dr Majewski started discussions with Dr Tai only recently about his potential involvement in the project, and due to lack of time we were not able to prepare a subcontract to Washington University, however Dr Tai agreed to assist us as a consultant. Dr Conti knows Dr Tai, his patented concepts are of interest to Siemens and therefore he will naturally fit into the team.

Progress conference calls are planned on bimonthly basis during the construction phase to review the status of the project and discuss new relevant developments in technology and science of the project. Once the systems will be transferred to Siemens, more often meetings will be organized at JHU during visits by the WVU team. Upon completion of the project, both PIs and their collaborators will make collective decision on potential publications and conference presentations of the summary results and on need and desire to submit new common proposals for continuation in the following projects with clinical trials included, and/or necessary upgrades of the apparatus. As appropriate, interim results and reports will be published or presented at conferences, as agreed by all collaborators.

**F. Addressing PCRP Overarching Challenges and Focus Areas**

We strongly believe that the goals of our proposal as explained above and in the attachments match very well the goals of FY10 PCRP program aimed towards eliminating death and suffering from prostate cancer through contribution to ***distinguishing lethal from indolent disease***, in part, due to the targeting of PSMA, which has proved the capability of providing a read-out on progressive disease (57)**.** Also, our submission is addressing two following PCRP focus areas: ***Biomarkers:*** Discovery and validation of biomarkers for the detection, prognosis, and progression of prostate cancer, and ***Imaging***: Development of new imaging technology for the detection and prognosis of prostate cancer, including progression to systemic disease.


1. Jemal, A., Murray, T., Samuels, A., Ghafoor, A., Ward, E., and Thun, M. J. (2003) Cancer statistics, 2003. *CA Cancer J Clin* **53**, 5-26.
2. Ghosh, A., and Heston, W. D. (2004) Tumor target prostate specific membrane antigen (PSMA) and its regulation in prostate cancer. *J Cell Biochem* **91**, 528-539
3. Mease, R. C., Dusich, C. L., Foss, C. A., Ravert, H. T., Dannals, R. F., Seidel, J., Prideaux, A., Fox, J. J., Sgouros, G., Kozikowski, A. P., and Pomper, M. G. (2008) N-[N-[(S)-1,3-Dicarboxypropyl]Carbamoyl]-4-[18F]Fluorobenzyl-L-Cysteine, [18F]DCFBC: A New Imaging Probe for Prostate Cancer. *Clin Cancer Res* **14**, 3036-3043
4. Vees, H., Buchegger, F., Albrecht, S., Khan, H., Husarik, D., Zaidi, H., Soloviev, D., Hany, T. F., and Miralbell, R. (2007) 18F-choline and/or 11C-acetate positron emission tomography: detection of residual or progressive subclinical disease at very low prostate-specific antigen values (<1 ng/mL) after radical prostatectomy. *BJU Int* **99**, 1415-1420
5. Testa, C., Schiavina, R., Lodi, R., Salizzoni, E., Corti, B., Farsad, M., Kurhanewicz, J., Manferrari, F., Brunocilla, E., Tonon, C., Monetti, N., Castellucci, P., Fanti, S., Coe, M., Grigioni, W. F., Martorana, G., Canini, R., and Barbiroli, B. (2007) Prostate cancer: sextant localization with MR imaging, MR spectroscopy, and 11C-choline PET/CT. *Radiology* **244**, 797-806
6. Dehdashti, F., Picus, J., Michalski, J. M., Dence, C. S., Siegel, B. A., Katzenellenbogen, J. A., and Welch, M. J. (2005) Positron tomographic assessment of androgen receptors in prostatic carcinoma. *Eur J Nucl Med Mol Imaging* **32**, 344-350
7. Larson, S. M., Morris, M., Gunther, I., Beattie, B., Humm, J. L., Akhurst, T. A., Finn, R. D., Erdi, Y., Pentlow, K., Dyke, J., Squire, O., Bornmann, W., McCarthy, T., Welch, M., and Scher, H. (2004) Tumor localization of 16beta-18F-fluoro-5alpha-dihydrotestosterone versus 18F-FDG in patients with progressive, metastatic prostate cancer. *J Nucl Med* **45**, 366-373
8. Carroll, P. R., Coakley, F. V., and Kurhanewicz, J. (2006) Magnetic resonance imaging and spectroscopy of prostate cancer. *Rev Urol* 8 Suppl 1, S4-S10
9. Jennifer S. Huber, William W. Moses, Jean Pouliot, and I.C. Hsu, *Dual-Modality PET/Ultrasound imaging of the Prostate*, Lawrence Berkeley National Laboratory. Paper LBNL-59114. (November 11, 2005), Huber, J.S.; Choong, W.S.; Moses, W.W.; Qi, J.; Hu, J.; Wang, G.C.; Wilson, D.; Oh, S.; Huesman, R.H.; Derenzo, S.E.; Budinger, T.F., Initial Results of a Positron Tomograph for Prostate Imaging, IEEE Transactions on Nuclear Science, Volume 53, Issue 5, Part 1, Oct. 2006 Page(s):2653 – 2659.
10. Turkington T.G.; Hawk, T.C.; Coleman, R.E.; Smith, M.F.; Majewski, S.; Kross, B.J.; Wojcik, R.; Weisenberger, A.G.; DeGrado, *PET prostate imaging with small planar detectors*, T.R. Nuclear Science Symposium Conference Record, 2004 IEEE Volume 5, Issue , 16-22 Oct. 2004 Page(s): 2806 – 2809.
11. Irving N. Weinberg, Valera Zavarzin, William Peter, Roberto Pani, JianChao Zeng, Pavel Stepanov, David Beylin, Edward Anashkin, Giuseppe DeVincentes, Lee P. Adler, Flexible Geometries for Hand-held PET and SPECT cameras, Nuclear Science Symposium and Medical Imaging Conference Record, 2002.

12. C. Levin, New Photon Sensor Technologies for PET in Prostate-Specific Imaging Configurations, presented at the Topical Symposium on *Advanced Molecular Imaging Techniques in the Detection, Diagnosis, Therapy, and Follow-Up of Prostate Cancer*, 6-7 December 2005, Rome, Italy, http://www.iss.infn.it/congresso/prostate/presentations_author.htm.
13. W. Moses, Dedicated PET Instrumentation for prostate imaging, presented at the Topical Symposium on *Advanced Molecular Imaging Techniques in the Detection, Diagnosis, Therapy, and Follow-Up of Prostate Cancer*, 6-7 December 2005, Rome, Italy, http://www.iss.infn.it/congresso/prostate/presentations_author.htm.
14. Sam S. Huh, Neal H. Clinthorne, and W. L. Rogers, Investigation of an internal PET probe for prostate imaging, Nucl. Instrum, Meth., 579, 339-343, 2007.
15. Yuan-Chuan Tai, Method and Apparatus for Increasing Spatial Resolution of a PET Scanner, US Patent 6.946,658 B2.
16. Yuan-Chuan Tai, Heyu Wu, and Martin Janecek, Initial Study of an Asymmetric PET System Dedicated to Breast Cancer Imaging, IEEE Trans. Nucl. Sci. 53, No. 1, 2006.
17. Yuan-Chuan Tai, Heyu Wu, Debashish Pal, and Joseph A. O'Sullivan, Virtual-Pinhole PET, J Nucl Med 2008; 49:471–479
18. Tae Yong Song, Heyu Wu, Sergey Komarov, Stefan B Siegel and Yuan-Chuan Tai, A sub-millimeter resolution PET detector module using a multi-pixel photon counter array, Phys. Med. Biol. 55 (2010) 2573–2587.
19. R.R. Raylman, S. Majewski, B. Kross, V. Popov, J. Proffitt, M.F. Smith, A.G. Weisenberger, R. Wojcik, Development of a Dedicated Positron Emission Tomography System for the Detection and Biopsy of Breast Cancer, Nuclear Instruments and Methods in Physics Research, A569 (2006), 291-295.
20. Raymond Raylman, Jame Abraham, Hannah Hazard, Cortney Coren, Shannon Filburn, Judith Schreiman, Stan Majewski, Gary Marano, Initial Clinical Test of a Breast-PET Scanner, submitted to Clinical Breast Cancer, 2010.
21. M. F. Smith, S. Majewski, A. G. Weisenberger, D. A. Kieper, R. R. Raylman, and T. G. Turkington, Analysis of factors affecting positron emission mammography (PEM) image formation, IEEE Trans. Nucl. Sci., vol. 50, pp. 53-59, 2003.
22. M. F. Smith and R. R. Raylman, PEM-PET image reconstruction in a clinically-relevant time frame, IEEE 2006 Nuclear Science Symposium Conference Record, pp. 1792-1796.
23. V. Popov, S. Majewski, B. L. Welch, A Novel Readout Concept for Multianode Photomultiplier Tubes with Pad Matrix Anode Layout Nuclear Instruments and Methods in Physics Research A 567 (2006) 319–322); V.Popov, US patent No: 6,747,263 B1.
24. Vladimir Popov, Stan Majewski, James Proffitt, John McKisson, Brian Kross, and Andrew Weisenberger, Study of Photonis XP1470 Nine-Channel Photomultiplier Tube For Applications in High Resolution Single Gamma and PET Imagers, presented at the 2007 IEEE MIC conference, Honolulu, Hawaii, October 27 – November 3, 2007.
25. M. Ritzert et al., "Compact SiPM based Detector Module for Time-of-Flight PET/MR." Realtime Conference, Beijing 2009.
26. T. Solf, et al. Solid-State Detector Stack for ToF-PET/MR. Nuclear Science Symposium and Medical Imaging Conference Record, 2009; 2798-2799.
27. V.C. Spanoudaki, et al. , Use of single photon counting detector arrays in combined PET/MR: Characterization of LYSO-SiPM detector modules and comparison with a LSO-APD detector." IOP Publishing Ltd 2007.
28. Hong, et al. An Investigation Into the Use of Geiger-Mode Solid-State Photomultipliers for Simultaneous PET and MRI Acquisition. IEEE Nucl Science Symposium Conf. Record 2008; 882-888.
29. J. Jung, Yong Choi, Key Jo Hong, Ji Hoon Kang, Wei Hu, Byung Jun Min, Yoon Suk Huh, Seung Han Shin, Hyun Keong Lim, Dae Shik Kim, and Han Byul Jin, MR Compatible Brain PET Using Tileable GAPD Arrays. 2009 IEEE Nuclear Science Symposium Conference Record, pp. 3556-3559.
30. K. J. Hong, Y. Choi, J. H. Kang, W. Hu, J. H. Jung, B. J. Min, H. K. Lim, S. H. Shin, Y. S. Huh, Y. H. Chung, P. Hughes and C. Jackson, Development of PET using 4 x 4 Array of Large Size Geiger-mode Avalanche Photodiodes, 2009 IEEE Nuclear Science Symposium Conference Record, pp. 3032-3037, Oct. 2009.
31. E. Heckathorne, Lanny Tiefer, Farhad Daghighian, and Magnus Dahlbom, Evaluation of Arrays of Silicon Photomultipliers for Beta Imaging, presented at the 2009 IEEE Nucl. Science Symposium and Medical Conf. Record 2009.
32. Proffitt, J.; Hammond, W.; Majewski, S.; Popov, V.; Raylman, R.R.; Weisenberger, A.G.; Wojcik, R. A flexible high-rate USB2 data acquisition system for PET and SPECT imaging. 2005 IEEE Nuclear Science Symposium Conference Record, Puerto Rico, October 23-29, 2005, pp. 2971-2975.
33. Proffitt, J., Hammond, W., Majewski, S.; Popov, V., Raylman, R.R., Weisenberger, A.G. Implementation of a High-Rate USB Data Acquisition System for PET and SPECT Imaging, 2006 IEEE Nuclear Science Symposium Conference Record, San Diego, California, October 29 – November 1, 2006, pp. 3063 - 3067.
34. J. E. McKisson, W. Hammond, J. Proffitt, and A.G. Weisenberger, A Java Distributed Acquisition System for PET and SPECT Imaging, 2007 IEEE Nuclear Science Symposium Conference Record, pp. 3591-3593.
35. F. Taghibakhsh, S. Cuddy, T. Rvachov, D. Green, A. Reznik, J. A. Rowlands, "Detectors with Dual-Ended Readout by Silicon Photomultipliers for High Resolution Positron Emission Mammography Applications", 2009 IEEE Nuclear Science Symposium Conference Record, pp. 2821-2826, Oct. 2009.
36. W.W. Moses, P.R.G Virador, S.E. Derenzo, R.H. Huesman, T.F. Budinger, "Design of a High Resolution, High-Sensitivity PET Camera for Human Brains and Small Animals", ", IEEE Transactions on Nuclear Science, Vol. 44, No. 4, August 1997.
37. Pomper, M. G., Musachio, J. L., Zhang, J., Scheffel, U., Zhou, Y., Hilton, J., Maini, A., Dannals, R. F., Wong, D. F., and Kozikowski, A. P. (2002) 11C-MCG: synthesis, uptake selectivity, and primate PET of a probe for glutamate carboxypeptidase II (NAALADase). *Mol Imaging* **1**, 96-101

38. Foss, C. A., Mease, R. C., Fan, H., Wang, Y., Ravert, H. T., Dannals, R. F., Olszewski, R., Heston, W. D., Kozikowski, A. P., and Pomper, M. G. (2005) Radiolabeled Small Molecule Ligands for Prostate-specific Membrane Antigen: In Vivo Imaging in Experimental Models of Prostate Cancer. *Clin Cancer Res* **11**, 4022-4028
39. Guilarte, T. R., McGlothan, J. L., Foss, C. A., Zhou, J., Heston, W. D., Kozikowski, A. P., and Pomper, M. G. (2005) Glutamate carboxypeptidase II levels in rodent brain using [125I]DCIT quantitative autoradiography. *Neurosci Lett* **387**, 141-144
40. Zhou, J., Neale, J. H., Pomper, M. G., and Kozikowski, A. P. (2005) NAAG peptidase inhibitors and their potential for diagnosis and therapy. Nat Rev Drug Discov 4, 1015-1026
41. Banerjee, S. R., Foss, C. A., Castanares, M., Mease, R. C., Byun, Y., Fox, J. J., Hilton, J., Lupold, S. E., Kozikowski, A. P., and Pomper, M. G. (2008) Synthesis and evaluation of technetium-99m- and rhenium-labeled inhibitors of the prostate-specific membrane antigen (PSMA). *J Med Chem* **51**, 4504-4517
42. Barinka, C., Byun, Y., Dusich, C. L., Banerjee, S. R., Chen, Y., Castanares, M., Kozikowski, A. P., Mease, R. C., Pomper, M. G., and Lubkowski, J. (2008) Interactions between human glutamate carboxypeptidase II and urea-based inhibitors: structural characterization. J Med Chem 51, 7737-7743
43. Chen, Y., Foss, C. A., Byun, Y., Nimmagadda, S., Pullambhatla, M., Fox, J. J., Castanares, M., Lupold, S. E., Babich, J. W., Mease, R. C., and Pomper, M. G. (2008) Radiohalogenated Prostate-Specific Membrane Antigen (PSMA)-Based Ureas as Imaging Agents for Prostate Cancer. *Journal of Medicinal Chemistry* **51**, 7933-7943
44. Chandran, S. S., Banerjee, S. R., Mease, R. C., Pomper, M. G., and Denmeade, S. R. (2008) Characterization of a targeted nanoparticle functionalized with a urea-based inhibitor of prostate-specific membrane antigen (PSMA). *Cancer Biol Ther* **7**, 974-982
45. Hillier, S. M., Maresca, K. P., Femia, F. J., Marquis, J. C., Foss, C. A., Nguyen, N., Zimmerman, C. N., Barrett, J. A., Eckelman, W. C., Pomper, M. G., Joyal, J. L., and Babich, J. W. (2009) Preclinical evaluation of novel glutamate-urea-lysine analogues that target prostate-specific membrane antigen as molecular imaging pharmaceuticals for prostate cancer. *Cancer Res* **69**, 6932-6940
46. Chen, Y., Dhara, S., Banerjee, S. R., Byun, Y., Pullambhatla, M., Mease, R. C., and Pomper, M. G. (2009) A low molecular weight PSMA-based fluorescent imaging agent for cancer. *Biochem Biophys Res Commun* **390**, 624-629
47. Maresca, K. P., Hillier, S. M., Femia, F. J., Barone, C., Joyal, J. L., Zimmerman, C. N., Barret, J. A., Foss, C. A., Eckelman, W. C., Pomper, M. G., and Babich, J. W. (2007) Molecular targeting of prostate cancer with small molecule inhibitors of prostate specific membrane antigen (PSMA). *Journal of Nuclear Medicine* **48**, 25
48. Mesters, J. R., Barinka, C., Li, W., Tsukamoto, T., Majer, P., Slusher, B. S., Konvalinka, J., and Hilgenfeld, R. (2006) Structure of glutamate carboxypeptidase II, a drug target in neuronal damage and prostate cancer. *Embo J* **25**, 1375-1384
49. Banerjee, S. R., Schaffer, P., Babich, J. W., Valliant, J. F., and Zubieta, J. (2005) Design and synthesis of site directed maleimide bifunctional chelators for technetium and rhenium. *Dalton Trans*, 3886-3897
50. Stephenson, K. A., Banerjee, S. R., Sogbein, O. O., Levadala, M. K., McFarlane, N., Boreham, D. R., Maresca, K. P., Babich, J. W., Zubieta, J., and Valliant, J. F. (2005) A new strategy for the preparation of peptide-targeted technetium and rhenium radiopharmaceuticals. The automated solid-phase synthesis, characterization, labeling, and screening of a peptide-ligand library targeted at the formyl peptide receptor. *Bioconjug Chem* **16**, 1189-1195
51. Stephenson, K. A., Banerjee, S. R., Besanger, T., Sogbein, O. O., Levadala, M. K., McFarlane, N., Lemon, J. A., Boreham, D. R., Maresca, K. P., Brennan, J. D., Babich, J. W., Zubieta, J., and Valliant, J. F. (2004) Bridging the gap between in vitro and in vivo imaging: isostructural Re and 99mTc complexes for correlating fluorescence and radioimaging studies. *J Am Chem Soc* **126**, 8598-8599
52. Banerjee, S. R., Levadala, M. K., Lazarova, N., Wei, L., Valliant, J. F., Stephenson, K. A., Babich, J. W., Maresca, K. P., and Zubieta, J. (2002) Bifunctional single amino acid chelates for labeling of biomolecules with the [Tc(CO)(3)](+) and [Re(CO)(3)](+) cores. Crystal and molecular structures of [ReBr(CO)(3)(H(2)NCH(2)C(5)H(4)N)], [Re(CO)(3)[(C(5)H(4)NCH(2))(2)NH]]Br, [Re(CO)(3)[(C(5)H(4)NCH(2))(2)NCH(2)CO(2)H]]Br, [Re(CO)(3)[X(Y)NCH(2)CO(2)CH(2)CH(3)]]Br (X = Y = 2-pyridylmethyl; X = 2-pyridylmethyl, Y = 2-(1-methylimidazolyl)methyl; X = Y = 2-(1-methylimidazolyl)methyl), [ReBr(CO)(3)[(C(5)H(4)NCH(2))NH(CH(2)C(4)H(3)S)]], and [Re(CO)(3)[(C(5)H(4)NCH(2))N(CH(2)C(4)H(3)S)(CH(2)CO(2))]]. *Inorg Chem* **41**, 6417-6425
53. Banerjee, S. R., Wei, L., Levadala, M. K., Lazarova, N., Golub, V. O., O'Connor, C. J., Stephenson, K. A., Valliant, J. F., Babich, J. W., and Zubieta, J. (2002) [Re(III)Cl(3)] core complexes with bifunctional single amino acid chelates. *Inorg Chem* **41**, 5795-5802
54. Velikyan, I., Maecke, H., and Langstrom, B. (2008) Convenient preparation of 68Ga-based PET-radiopharmaceuticals at room temperature. *Bioconjug Chem* **19**, 569-573
55. Banerjee, S. R., Foss, C.A., Castanares, M., Mease, R.C., Byun, Y., Fox, J.J., Hilton, J., Lupold, S., Kozikowski, A.P., Pomper, M.G. (in press) Synthesis and evaluation of technetium-99m- and rhenium-labeled inhibitors of the prostate-specific membrane antigen (PSMA). *J. Med. Chem.*
56. McBride, W. J., Sharkey, R. M., Karacay, H., D'Souza, C. A., Rossi, E. A., Laverman, P., Chang, C. H., Boerman, O. C., and Goldenberg, D. M. (2009) A novel method of 18F radiolabeling for PET. *J Nucl Med* **50**, 991-998
57. Perner S, Hofer MD, Kim R, Shah RB et al., Prostate-specific Membrane Antigen Expression as a Predictor for Prostate Cancer Progression. Human Pathology 2007; 38:696-701